

# *Bacteroides* expand the functional versatility of a conserved transcription factor and transcribed DNA to program capsule diversity

Received: 2 July 2024

Accepted: 2 December 2024

Published online: 30 December 2024

Jason Saba<sup>1,2</sup>, Katia Flores<sup>3,4</sup>, Bailey Marshall<sup>1,5</sup>, Michael D. Engstrom<sup>1</sup>, Yikai Peng<sup>1</sup>, Atharv S. Garje<sup>1,6</sup>, Laurie E. Comstock<sup>3,4</sup> & Robert Landick<sup>1,7</sup> 

The genomes of human gut bacteria in the genus *Bacteroides* include numerous operons for biosynthesis of diverse capsular polysaccharides (CPSs). The first two genes of each CPS operon encode a locus-specific paralog of transcription elongation factor NusG (called UpxY), which enhances transcript elongation, and a UpxZ protein that inhibits noncognate UpxYs. This process, together with promoter inversions, ensures that a single CPS operon is transcribed in most cells. Here, we use in-vivo nascent-RNA sequencing and promoter-less in-vitro transcription (PIVoT) to show that UpxY recognizes a paused RNA polymerase via sequences in both the exposed non-template DNA and the upstream duplex DNA. UpxY association is aided by ‘pause-then-escape’ nascent RNA hairpins. UpxZ binds non-cognate UpxYs to directly inhibit UpxY association. This UpxY-UpxZ hierarchical regulatory program allows *Bacteroides* to generate subpopulations of cells producing diverse CPSs for optimal fitness.

*Bacteroides* are abundant and crucial members of the modern human gut microbiota. A key evolved feature of these bacteria is the ability of each strain to produce numerous (eight or more) distinct capsular polysaccharides (CPS)<sup>1,2</sup> that are tightly regulated so that only one CPS is typically produced per bacterial cell. This bet-hedging strategy generates *Bacteroides* populations with great surface variability that protect from phage<sup>3–5</sup> and mediate immune modulation, biofilm formation, antibiotic resistance, and inflammation<sup>6–11</sup>.

CPS diversity is achieved by regulating both transcription initiation and elongation of CPS biosynthesis operons. *Bacteroides fragilis* (*Bfr*) has eight distinct CPS operons, producing PSA–PSH. All but PSC use invertible promoters and all encode *upxY* ( $Y_X$ ) and *upxZ* ( $Z_X$ ) paralogs as the first genes in each operon<sup>12,13</sup>. The fraction of each

promoter oriented ON versus OFF varies with environmental conditions<sup>14</sup>. CPS promoter inversions are stochastic and multiple CPS promoters are oriented ON in most cells simultaneously<sup>15–17</sup>. *Bacteroides* prioritize expression of one promoter-ON CPS operon over others by regulating RNA polymerase (RNAP) elongation via the operon-specific  $Y_X$  elongation activator and  $Z_X$  inhibitor of non-cognate  $Y_X$ .  $Z_X$  inhibits a subset of non-cognate  $Y_X$  possibly via direct binding (e.g.,  $Z_A$  from PSA may inhibit  $Y_E$  from PSE). *Bfr*  $Y_X$  paralogs must distinguish among eight target CPS loci to enable operon-specific regulation, but how this discrimination is accomplished is unknown.

$Y_X$  family proteins are specialized (i.e., locus-specific) paralogs of NusG/Spt5, the only universal transcription factor found in archaea, eukaryotes, and bacteria<sup>18</sup>. NusG-family regulators bind RNAPs during

<sup>1</sup>Department of Biochemistry, University of Wisconsin–Madison, Madison, WI, USA. <sup>2</sup>Microbiology Doctoral Training Program, University of Wisconsin–Madison, Madison, WI, USA. <sup>3</sup>Department of Microbiology, University of Chicago, Chicago, IL, USA. <sup>4</sup>Duchossois Family Institute, University of Chicago, Chicago, IL, USA. <sup>5</sup>Cell and Molecular Biology Training Program, University of Wisconsin–Madison, Madison, WI, USA. <sup>6</sup>Genetics Training Program, University of Wisconsin–Madison, Madison, WI, USA. <sup>7</sup>Department of Bacteriology, University of Wisconsin–Madison, Madison, WI, USA.

 e-mail: [rlandick@wisc.edu](mailto:rlandick@wisc.edu)

transcript elongation and modulate RNAP activity through interactions with the RNAP and the surface-exposed ntDNA strand<sup>19–21</sup>. Globally acting *Escherichia coli* NusG and its single specialized paralog RfaH increase elongation rate and decrease pausing<sup>22–25</sup>. In contrast, *Bacillus subtilis*, *Mycobacterium tuberculosis*, and *Thermus thermophilus* NusGs enhance both pausing and intrinsic termination<sup>26–30</sup>. Pausing during transcript elongation is a universal regulatory feature of RNAPs that allows site-specific recruitment of transcription factors (TFs)<sup>31</sup> and guides RNA synthesis.

Among the known NusG<sub>SP</sub> families, RfaH of Proteobacteria is the best understood. RfaH targets operons that contain a DNA element

called *ops* (operon polarity suppressor) in their leader regions (DNA between the transcription start site and the translation start codon of the first gene). RNAP pauses at the 12-nucleotide *ops*, allowing RfaH to associate via sequence-specific interactions with a non-template strand DNA hairpin (ntDNAhp) exposed by the paused RNAP<sup>22,23,32,33</sup>. Other NusG<sub>SP</sub> include LoqP in Firmicutes<sup>21</sup>, TaA in Myxococcota<sup>34</sup>, and plasmid-encoded ActX in Proteobacteria<sup>35</sup>.

The CPS operon leader regions are required for Y-mediated regulation<sup>12</sup>, consistent with sequence-specific Y<sub>X</sub> recruitment to RNAP paused in this region (Fig. 1a). In principle, Y<sub>X</sub> could recognize ntDNA (like RfaH), nascent RNA (like LoqP), or both to discriminate among

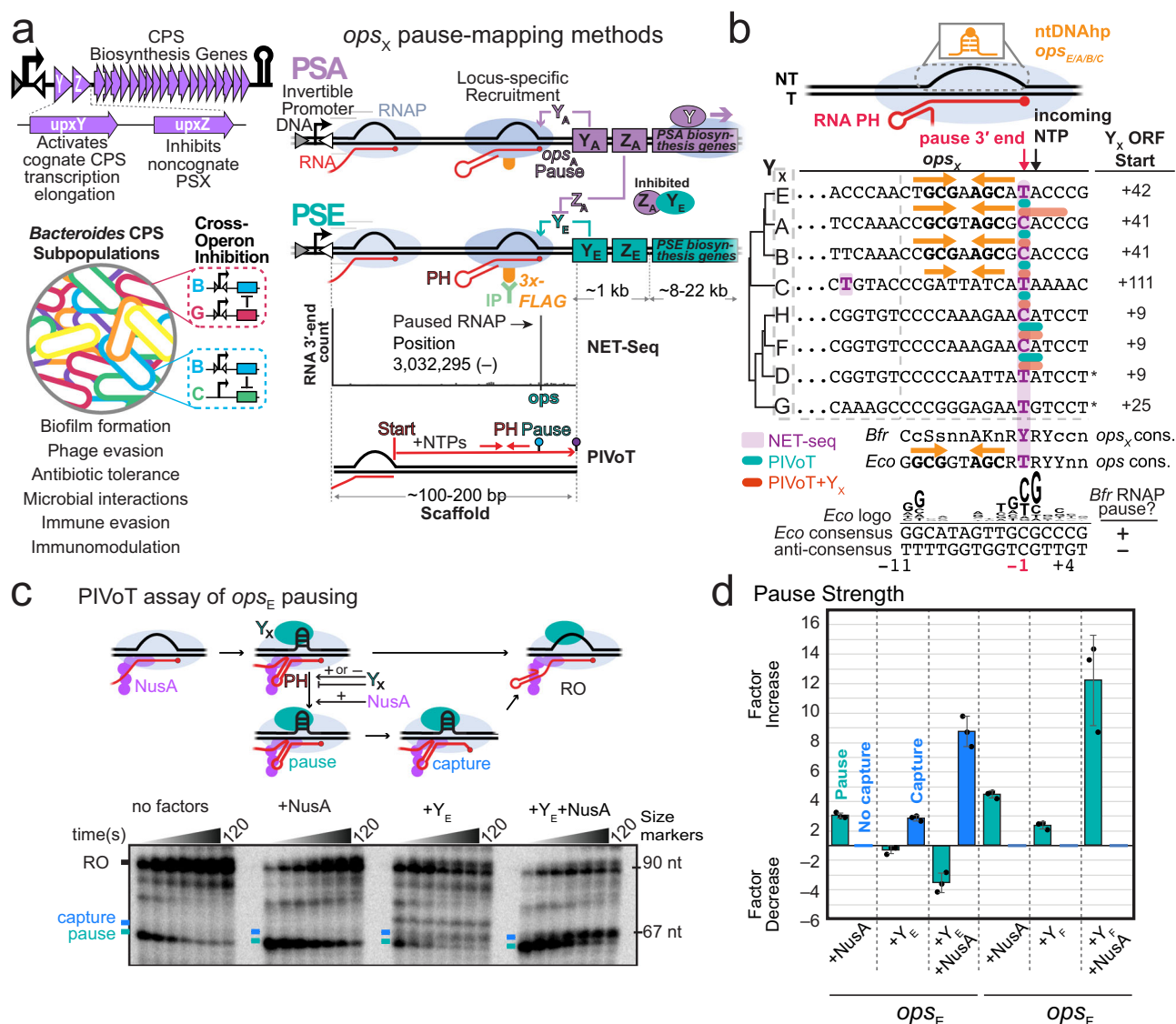


**Fig. 1 | *Bacteroides fragilis* RNAP pauses in CPS operon leader regions in vivo and in vitro at candidate Y<sub>X</sub> recruitment sites called *ops<sub>X</sub>*.** **a** Representative CPS operon diagram highlighting Y<sub>X</sub> and Z<sub>X</sub>, the first two genes in *B. fragilis* PSX operons. Horizontal triangles mark the inverted repeats recognized by Mpi recombinase for promoter inversion<sup>17</sup>. Proposed roles for CPS diversity in *B. fragilis* subpopulations (colored coats) are listed<sup>3,6,8–10,99</sup>. The schematics illustrate the proposed roles of Y<sub>X</sub> activation and Z<sub>X</sub> inhibition of noncognate Y<sub>X</sub> in generating subpopulation CPS diversity<sup>12,13</sup>. Y<sub>X</sub> is recruited to RNAP paused at cognate but not non-cognate *ops<sub>X</sub>* sites that encode a pause hairpin (PH). Z<sub>X</sub> directly binds Y<sub>X</sub> from heterologous operons and inhibits its recruitment. In vivo (NET-seq) and in vitro (PIVoT) methods for identifying RNAP pause sites (*ops<sub>X</sub>*) are illustrated.

**b** Transcriptional pauses in CPS leader regions identified in this study are shown in

comparison to the RfaH *ops* pause and the *E. coli* consensus elemental pause sequences<sup>37</sup>. T template strand, NT non-template strand. Fully conserved nucleotides are capitalized; largely conserved nucleotides are lowercase. Asterisks (\*) indicate operons were only probed in vivo. **c** PIVoT assay of PSE promoter-distal leader regions. Assays included 1 μM NusA or 150 nM Y<sub>E</sub> added concomitantly with NTPs as indicated. RNAs from a reaction time course were separated by 8% Urea-PAGE. **d** NusA and Y<sub>X</sub> synergistic activities at cognate *ops<sub>X</sub>* sites. Y<sub>X</sub> association manifests as pause inhibition or pause enhancement (aqua bars), or capture (blue bars). Fold changes in pausing or capture (if applicable) after addition of factors are shown relative to baseline (no factors control). Data are presented as mean values ± SD from *n* = 3 independent experiments.

multiple, similar CPS operon targets. We used both in vivo and in vitro analyses to identify pauses in CPS operon leader regions, establish that these pause sites function as recruitment sites for Y, and discover NusG<sub>SP</sub>-DNA interactions and mechanisms that mediate Y-CPS operon specificity. We found that Z directly binds noncognate Ys to block Y action and that differential Y<sub>X</sub>-Z<sub>X</sub> affinities enable CPS hierarchical control of transcript elongation. These results define mechanisms that explain the exquisite specificity of multiple NusG<sub>SP</sub> and that allow *Bacteroides* to program CPS diversity in the highly dynamic human gut environment.

## Results

### *Bacteroides fragilis* RNAP pauses in CPS operon leader regions in vivo and in vitro at candidate Y<sub>X</sub>-recruitment sites (*ops<sub>X</sub>*)

Specific Y<sub>X</sub> recruitment sites likely exist in CPS leader regions because these leader sequences are variable and are required for Y<sub>X</sub> activity<sup>12</sup>. Since *EcoRfaH* is recruited to RNAP at leader region *ops* pause sites, we first asked if *Bfr*RNAP pauses in the leader regions of CPS operons. To identify candidate Y<sub>X</sub>-recruiting pause sites directly in vivo, we used nascent elongating transcript sequencing (NET-seq) (Fig. 1a, b and Supplementary Fig. 1a). NET-seq allows genome-scale identification of precise nascent RNA 3' ends, which are enriched at pause sites<sup>36,37</sup>.

NET-seq revealed single prominent pause sites in most CPS operon leader regions (Fig. 1a, b and Supplementary Fig. 1b)<sup>37</sup>. Eight CPS leader pauses exhibited an obvious consensus sequence that resembles strong *E. coli* pauses (Fig. 1b) as well as apparent nascent RNA pause hairpins (PHs) that resemble those known to enhance pausing allosterically in concert with NusA in other bacteria (e.g., the so-called type-1 *E. coli* *his* and *B. subtilis* *trp* leader region pauses; Supplementary Fig. 1c)<sup>37–40</sup>. Pausing in the PSC leader region (the only *Bfr* CPS operon with a non-invertible, constitutively ON promoter)<sup>41</sup> occurred at multiple sites; weak pausing occurred at a site resembling the other seven in sequence and location (Fig. 1b and Supplementary Fig. 1b). We designated the CPS leader pause sites *ops<sub>X</sub>* ('X' designates the CPS operon) based on analogy to the RfaH *ops* site.

To test whether the *ops<sub>X</sub>* pause recruits Y<sub>X</sub>, we generated recombinant *Bacteroides fragilis* RNAP (*rBfr*RNAP) and assayed CPS leader regions using promoter-less in vitro transcription (PIVoT) (Fig. 1a and Supplementary Fig. 2a, b)<sup>42,43</sup>. PIVoT bypasses the need for σ<sup>A</sup>-dependent initiation. We first asked if *rBfr*RNAP recognizes the consensus elemental pause signal defined for *Eco*RNAP (Fig. 1b)<sup>37</sup>. Signals resembling this consensus direct pausing by a wide variety of RNAPs from bacteria to human<sup>37,44,45</sup>. Bacterial pause sequences are reported to differ in some species<sup>46,47</sup> and have not been tested for Bacteroidota. We found that *rBfr*RNAP pauses strongly at the consensus sequence but not anti-consensus sequence (Supplementary Fig. 2c), suggesting its pause signals resemble those of *Eco*RNAP and most other tested RNAPs.

We next assayed pausing in for six of the eight CPS leader regions (PSA, B, C, E, F, and H). Strikingly, the PSA, B, E, F, and H leader segments encoded prominent pause sites that corresponded exactly to the sites found by NET-seq (Supplementary Figs. 2d, 3). Pausing was less prominent but detectable at *ops<sub>C</sub>*, consistent with the heterogeneous pausing observed the NET-seq. We conclude that CPS operon leader regions encode strong pause sites for RNAP with similar but not identical sequences, as might be expected for Y<sub>X</sub> recruitment sites that must distinguish among Y<sub>X</sub> paralogs.

To ask if the CPS leader pauses function as targets for Y<sub>X</sub> recruitment and test whether they are modulated by regulators like NusA and Y<sub>X</sub>, we purified recombinant *Bfr*NusA and Y<sub>X</sub> for these six PSA operons (Y<sub>A</sub>, Y<sub>B</sub>, Y<sub>C</sub>, Y<sub>E</sub>, Y<sub>F</sub>, and Y<sub>H</sub>; Methods) and tested their effects on pausing using PIVoT. In *Eco* and *Bsu*, NusA stimulates pausing in part via contacts to PHs<sup>37,39,43,48–50</sup>. All six CPS leader pauses were greatly enhanced by NusA (Fig. 1c and Supplementary Fig. 4). Intriguingly, Y<sub>A,B,E</sub> inhibited the cognate leader pause, whereas Y<sub>C,F,H</sub>

enhanced the cognate leader pause (Fig. 1c, d and Supplementary Fig. 4). Y<sub>E</sub> additionally trapped a fraction of RNAP just downstream from the pause site, as seen previously with *Eco*RfaH ('capture' in Fig. 1c, d and Supplementary Fig. 4). Thus, Y<sub>X</sub> association with paused elongation complexes (PECs) may manifest as either pro-pausing or anti-pausing activity.

Importantly, the effects of Y<sub>X</sub> are likely to be specific to the NET-seq identified leader pauses, consistent with *ops<sub>X</sub>* sites functioning as specific Y<sub>X</sub>-recruitment sites. Y<sub>X</sub> only modulated pausing at cognate *ops<sub>X</sub>* but not non-cognate *ops<sub>X</sub>* or other positions (Supplementary Fig. 4). We conclude that the NET-seq-identified leader pauses are bona fide target sites for Y<sub>X</sub> association with *Bfr*RNAP. Notably, *ops<sub>A,B,E</sub>* encode putative ntDNAhps at [−11 to +1] that resemble the *ops* ntDNAhp known to recruit *Eco*RfaH (5'-GCG-AGC stems; Fig. 1b and Supplementary Fig. 1c). The *Bfr ops<sub>X</sub>* ntDNAhp sequences differ, consistent with specific recruitment of cognate Y<sub>X</sub>. However, *ops<sub>F,H</sub>* are identical in the ntDNAhp region, suggesting that some other element contributes to specificity.

RNAP capture by Y<sub>X</sub>-*ops<sub>X</sub>* interaction, which is evident by accumulation of RNAs a few nucleotides longer than the primary pause RNA for *ops<sub>E</sub>* but not *ops<sub>A</sub>* or *ops<sub>B</sub>* (Supplementary Fig. 4), suggests some but not all *ops<sub>X</sub>* sites exhibit pause cycling<sup>31,33,51</sup>. Pause cycling occurs when the ntDNA is captured by a regulator that also contacts RNAP (e.g., *Eco*<sup>70</sup> or RfaH), anchoring the PEC and hindering extension beyond 2–3 nt<sup>52,53</sup>. Trapped PECs can be rescued by RNA cleavage factors GreA,B<sup>33</sup>, creating a cycle that repeats until ntDNA contacts rearrange to allow normal elongation<sup>51</sup>.

Importantly, even in the presence of globally acting *Bfr*NusG, Y<sub>E</sub> still enhances *ops<sub>F</sub>* pausing (Supplementary Fig. 5a). Thus, Y<sub>X</sub> appears to outcompete *Bfr*NusG even though both NusG and its specialized paralog Y<sub>X</sub> use the same primary binding site on RNAP (Supplementary Fig. 5b).

### Z<sub>X</sub> inhibits Y<sub>X</sub> at *ops<sub>X</sub>* through direct Z<sub>X</sub>-Y<sub>X</sub> interaction

We next sought to test whether Y<sub>X</sub> binding requires sequence upstream of the putative ntDNAhp region using in vitro binding, in silico interaction, and in vivo gene expression assays. Y<sub>E</sub> is predicted to be inhibited by Z<sub>A</sub> but not by Z<sub>E</sub> or Z<sub>C</sub> in a strain with only the PSA, PSE, and PSC promoters oriented ON (expression hierarchy PSA > E > C)<sup>13,17</sup>. We call this strain [AE]<sub>ON</sub> for simplicity because the PSC promoter is constitutive<sup>13</sup>. To test our prediction, we measured Z<sub>A</sub>-Y<sub>E</sub> and Z<sub>E</sub>-Y<sub>E</sub> binding constants by biolayer interferometry (BLI) (Fig. 2a, b). Z<sub>A</sub> but not Z<sub>E</sub> bound tightly to Y<sub>E</sub> (*K<sub>D</sub>* - 0.9 nM vs -88 nM). We conclude that Z<sub>X</sub> acts through direct Y<sub>X</sub> binding.

To understand how Z<sub>A</sub> might interact with Y<sub>E</sub>, we predicted their association using AlphaFold 3<sup>54</sup> (Fig. 2c and Supplementary Fig. 6). The Z<sub>A</sub>-Y<sub>E</sub> complex, which was predicted with high confidence, placed Z<sub>X</sub> on the RNAP-binding interface of Y<sub>E</sub>. When modeled into an *Eco*RNAP-RfaH-*ops*-PEC (PDB 8PHK)<sup>33</sup> by alignment of the Y<sub>E</sub> NGN domain with the RfaH NGN, Z<sub>A</sub> clashed with two major PEC features: (i) the RNAP clamp helices (CH), which provide the primary RNAP binding site for all NusG-family regulators (Fig. 2c, orange); and (ii) the proximal upstream DNA duplex (usDNA). Thus, Z<sub>X</sub> likely inhibits Y<sub>X</sub> by preventing its recruitment to RNAP at *ops<sub>X</sub>* pause sites.

We next used PIVoT to test whether Z<sub>A</sub> or Z<sub>E</sub> blocked Y<sub>E</sub> inhibition of pausing at the candidate *ops<sub>E</sub>* pause site as predicted by the AlphaFold model. Z<sub>E</sub> blocked Y<sub>E</sub> action only at high concentrations (*K<sub>i</sub>* approximating the *K<sub>D</sub>* measured by BLI; Fig. 2d). In contrast, Z<sub>A</sub> inhibited Y<sub>E</sub> at all tested concentrations. We conclude that differential Y<sub>X</sub>-Z<sub>X</sub> affinities enable CPS hierarchical control of transcript elongation (Fig. 2e).

### Y<sub>X</sub> targets extended *ops<sub>X</sub>* sites in vivo

Using these insights into Z<sub>X</sub>-Y<sub>X</sub> interaction, we tested whether *ops<sub>X</sub>* pause sites function as Y<sub>X</sub> recruitment sites in vivo and which

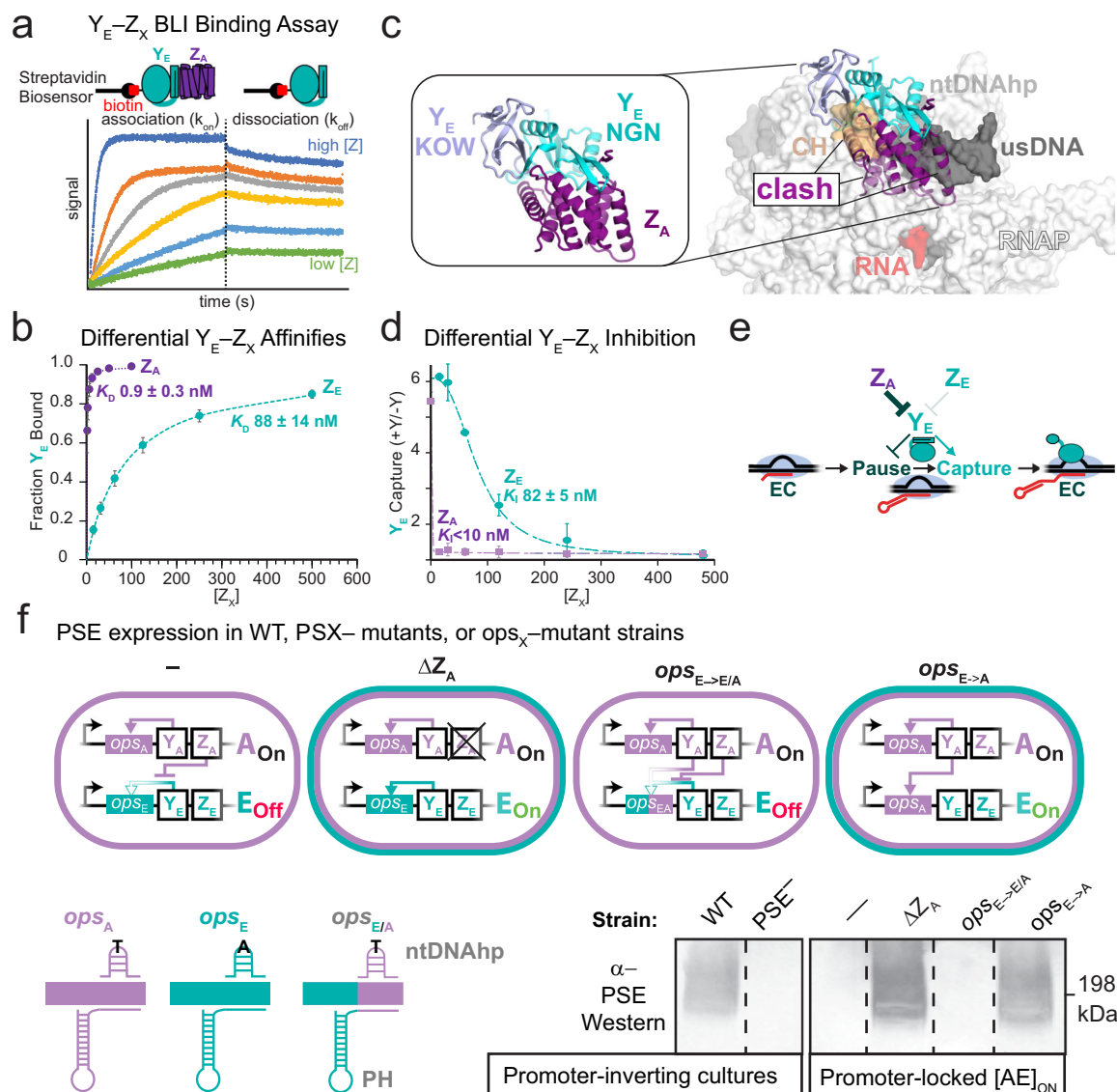


**Fig. 2 |  $ops_X$  pause sites are recruitment sites in vivo that enable  $Y_X$ -locus specificity, CPS hierarchical control, and can be re-wired to bypass direct inhibition by  $Z_X$ .** **a**  $Z_X$  directly binds  $Y_X$  as revealed by biolayer interferometry (BLI<sup>100</sup>) over a range of  $Z_X$  concentrations yielding biotin- $Y_E$ - $Z_X$  on and off rates:  $Y_E$ - $Z_A$   $k_{on} = 1.1 \times 10^6 \pm 2.9 \times 10^5$  M<sup>-1</sup>s<sup>-1</sup>,  $k_{off} = 9.0 \times 10^{-4} \pm 2.4 \times 10^{-4}$  s<sup>-1</sup>;  $Y_E$ - $Z_E$   $k_{on} = 1.1 \times 10^5 \pm 2.5 \times 10^4$  M<sup>-1</sup>s<sup>-1</sup>,  $k_{off} = 9.6 \times 10^{-3} \pm 7.3 \times 10^{-4}$  s<sup>-1</sup>. Assays were performed in triplicate and globally fit to a 1:1 binding model (see Methods). Reported  $K_D$ s are averages from three independent global fits and errors represent standard deviations. **b**  $Y_E$ - $Z_A$  and  $Y_E$ - $Z_E$  binding curves. The control group used buffer in place of  $Z_X$  and was subtracted from all binding curves shown (see Methods). Data are presented as mean values  $\pm$  SD from  $n = 3$  independent experiments. **c** AlphaFold<sup>34</sup> model of  $Y_E$ - $Z_A$  and steric clash evident when  $Y_E$ - $Z_A$  is aligned to an RfaH-bound PEC<sup>23</sup>. **d** Fold changes in  $Y_E$  capture as a function of cognate  $Z_E$  or non-cognate  $Z_A$

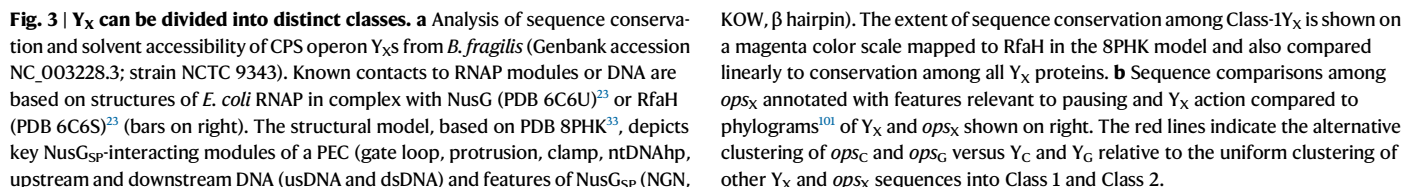
concentration in PIVOt assays (Methods). Subsets of NusA,  $Y_E$ , variable  $[Z_X]$ , and NTPs were added to initiate pause assays (50 nM  $Y_E$ , 15–480 nM  $Z_X$ , 1  $\mu$ M NusA, final). The control group used buffer in place of  $Z_X$  and was subtracted from all binding curves shown (see Methods). Data are presented as mean values  $\pm$  SD from  $n = 3$  independent experiments. **e** Model for  $Z_X$  inhibition of  $Y_X$  recruitment. **f** Strain background used in  $ops_X$  replacement experiments are depicted ( $\Delta mpi$  M44 in each strain ensured only the PSA, PSC, and PSE promoters are oriented ON). In WT, promoter orientations are variable in single cells, but some cells express PSE. PSE<sup>-</sup> is an insertion mutant that abrogates PSE expression. In promoter-locked  $[AE]_{ON}$  strains, only  $Y_A$ -activated genes are expressed because of cross-operon inhibition of  $Y_E$  and  $Y_C$  by  $Z_A$ . Strains with partial  $[-10:-1]_E$  or full  $[-38:-1]_E$  segments of  $ops_E$  were replaced with their  $ops_A$  counterparts ( $[-10:-1]_A$  and  $[-43:-1]_A$ ) and assayed for their ability to rescue PSE expression by Western blot.

sequences govern cognate  $Y_X$  function. Using a constitutive  $[AE]_{ON}$  strain<sup>17</sup>, we replaced  $ops_E$  segments with the corresponding  $ops_A$  segments. We predicted that the  $ops_E$ - $ops_A$  swapped strain should activate PSE expression because  $Y_A$  should bind  $ops_A$  in PSE. To ask if the PH-encoding region of  $ops_X$  is required for  $Y_X$  recruitment, we also constructed a hybrid  $ops_{E \rightarrow A}$  strain in which only the ntDNAhp region corresponding to the RfaH  $ops$  but not the PH-encoding region of  $ops_E$  was replaced with  $ops_A$  sequence (Fig. 2f). Using antibodies confirmed to detect PSE in a WT strain but not in a PSE<sup>-</sup> mutant, we tested for PSE

expression in  $[AE]_{ON}$  and derivative strains:  $\Delta Z_A$ , hybrid  $ops_{E \rightarrow A}$ , and full  $ops_{E \rightarrow A}$  (Fig. 2f). PSE was (i) not expressed in  $[AE]_{ON}$ ; (ii) expressed in  $\Delta Z_A$ ; (iii) not expressed in the hybrid  $ops_{E \rightarrow A}$  strain; and expressed in the full  $ops_{E \rightarrow A}$  swapped strain.

To confirm that the upstream PH-encoding region is required for  $Y_X$  action, we also tested  $Y_A$  and  $Y_E$  effects similarly using PIVOt (Supplementary Fig. 7a, b). Neither  $Y_A$  nor  $Y_E$  modulated pausing or PEC capture at WT levels unless the full cognate  $ops_X$  including the upstream PH-encoding region was present. Thus, both in vivo and





The Class-1 PSA,B PHs have greater potential to extend towards the pause RNA 3' end (teal highlight) relative to the PSE PH. Extension of PHs past -10 is thought to destabilize PECs at intrinsic terminators<sup>88</sup>, but we did not observe termination at these sites. An alternative role of PHs extending past -10 could be to aid PEC escape from pause cycles if auxiliary factors like GreA,B are insufficient. Thus, we postulated that base-pairing of the PSA,B PHs at -11, -10, and -9 could explain why, in contrast to  $Y_F$ ,  $Y_A$ , and  $Y_B$  did not capture PECs in pause cycles

(Supplementary Fig. 4 and Fig. 3b red highlight) (see next section). Based on an apparent ability to prevent PEC capture by  $Y_X$ , we call this PH extension the escape duplex (ED).

Pro-pausing Class-2 (PSD,F,H) sequences exhibited features that differed from Class-1 (Fig. 3b and Supplementary Fig. 8). For Class-2 DNA-RNA: (i)  $ops_X$  lacks an obvious ntDNAhp; (ii) the apparent PH extends only to -14; and (iii) the  $Y_X$  gene start codon is at +9 relative to  $ops_X$ . For Class-2  $Y_X$ : (i) the  $\beta 2$ - $\beta 3$  hairpin sequence is variable with pattern of basic residues distinct from Class-1; (ii) NGN  $\alpha 1$  and  $\alpha 2$  also are variable but distinct from Class-1 and thus consistent with differential recognition and different effects on pausing; and (iii) the KOW domain exhibits greatly increased positive charge relative to Class-1 (Supplementary Fig. 8).

PSC,G were outliers whose  $Y_X$  and  $ops_X$  clustered differently relative to Class-1,2. Their apparent PHs extended to -12 or -16, respectively. The  $Y_X$  start codons were at +111, +25 and both  $Y_X$  sequences were relatively divergent compared to Class-1,2.  $Y_C$  enhanced rather than inhibited the  $ops_C$  pause (Supplementary Fig. 4). Class-2  $Y_X$  and PSC  $Y_C$  exhibited charge similarity to the Loaf KOW proposed to bind RNA hairpins (Supplementary Fig. 8).

We conclude that  $Y_X$  regulators diverged during evolution to form at least two distinct classes within which the interactions that determine  $Y_X$ - $ops_X$  specificity and pro- vs. anti-pausing action appear to have followed different trajectories.

### **$ops_X$ PHs stabilize PECs but also can aid escape of PECs captured by $Y_X$ -DNA contacts**

We next sought to assess the function of the putative  $ops_X$  PHs (Fig. 3b). We focused on Class-1  $ops_X$  to investigate the impact of the PH and ED (Fig. 3b and Supplementary Fig. 9). The strong effect of NusA on Class-1 pauses (Fig. 1d and Supplementary Fig. 4) made it likely the PHs stimulate pausing<sup>39,43,48–50,59</sup>. Further, removal of the PH-encoding region from an  $ops_E$  scaffold eliminated NusA-stimulation of pausing (Supplementary Fig. 10a). To probe the functions of the conventional  $ops_E$  PH and the unconventional  $ops_B$  PH + ED, we used complementary antisense oligonucleotides (asDNAs or asRNAs) to progressively disrupt the 5' arm of the PSE,B PHs (Fig. 4a, c).

asDNAs that disrupt the PSE PH by pairing with the 5' arm, but not those that pair just upstream, reduced pausing (Fig. 4b). Thus, the PH alone stimulates pausing at  $ops_X$  and *Bfr*NusA significantly stimulates pausing in a PH-dependent manner. We conclude that  $ops_X$  sites are type-1 pauses that encode NusA-stabilized PHs, in notable contrast to the type-2 RfaH  $ops$  that lacks a PH<sup>38</sup>.

To test the idea that the apparent ED could aid escape of PECs, we measured the effect on capture of antisense RNAs (asRNAs) that disrupt the ED by pairing to the distal bases of 5' arm of the  $ops_B$  PH.  $ops_B$  but not  $ops_E$  encodes an ED, and  $Y_B$  does not cause PEC capture in contrast to  $Y_E$  (Fig. 4c, d and Supplementary Fig. 4). Addition of asRNAs that progressively disrupted the ED caused  $Y_B$  to capture PECs in pause cycles. Thus,  $ops_B$ , and by analogy  $ops_X$ , PHs not only stimulate  $ops_X$  pausing synergistically with NusA to allow time for  $Y_X$  recruitment, but also use an ED to drive forward translocation at the pause. The ED breaks extensive contacts by  $Y_X$  necessary for its initial recruitment but problematic for subsequent EC escape.

### **$Y_X$ distinguishes PECs via multipartite NGN interactions with exposed ntDNA and upstream duplex DNA**

We next sought to determine how Class-1  $Y_X$  proteins distinguish cognate vs. non-cognate  $ops_X$  sites via the PH-encoding region (Fig. 2). Since the ntDNA of  $ops_E$  and  $ops_B$  are most similar, particularly at the key -6 ntDNAhp position (Fig. 3b and Supplementary Fig. 10b), we reasoned that the contribution of sequences upstream from the ntDNAhp might be most apparent by swapping regions between  $ops_E$  and  $ops_B$ . We used PIVoT to measure  $Y_X$  effects on NusA-stimulated pausing and capture using templates with  $ops_{E-B}$  swapped sequences

or  $Y_E$ - $Y_B$  hybrid proteins that separate potential NGN vs. KOW contributions (Fig. 5a). To enable the direct comparison between  $ops_E$  and  $ops_B$ , we used a variant of  $ops_B$  that lacked the ED ( $ops_{B,-ED}$ ).

To ask if  $Y_X$  recognizes the upstream DNA or the PH RNA encoded by it, we first tested whether the upstream DNA sequences affected  $Y_X$  action in the absence of a PH (Fig. 5b). With the PH removed,  $Y_B$  stimulated RNAP capture at the  $ops_B$  pause site by a factor of ~4.5 (Fig. 5c). When 3-bp segments of the  $ops_B$  usDNA were replaced with  $ops_E$  sequence,  $Y_B$  capture of RNAP decreased either modestly (substitutions 1 and 2) or nearly completely (substitution 3). We next asked if changing both the upstream DNA and the PH from  $ops_B$  to  $ops_E$  sequences had more effect on  $Y_B$  action than changing just the upstream DNA, as predicted if the PH functions in  $Y_B$  action. However, even combining the 1 + 2 + 3 substitutions in the upstream DNA and PH had no greater defect in  $Y_B$  action than introducing substitution 3 to the upstream DNA alone (Fig. 5d). We conclude that  $Y_B$  recognition of the extended  $ops_B$  site depends on the usDNA and not on the PH RNA.

We next investigated the contributions of the upstream sequences in progressively interconverted  $ops_E$  and  $ops_B$  to PEC capture by  $Y_X$  (Fig. 5e and Supplementary Fig. 11). To simplify this comparison, we used a variant of  $ops_B$  in which capture was activated by removing the ED (Supplementary Figs. 9, 11). Strikingly,  $Y_E$  continued to function even when the  $ops_E$  ntDNAhp was changed to the  $ops_B$  ntDNAhp. However, the  $Y_E$  effect was mostly lost and  $Y_B$  capture progressively increased as the usDNA was increasingly converted to  $ops_B$  sequence (Fig. 5e). Thus, multiple segments of usDNA contribute to  $Y_B$  recognition of  $ops_B$ . Consistent with our in vivo experiments (Fig. 2f), we conclude that  $ops_X$  sequences are multipartite ntDNA and usDNA signals of ~40 nucleotides whose constituent parts variably contribute to  $Y_X$  recruitment in different CPS operons.

We next asked if the NGN alone recognizes  $ops_X$  as it does for RfaH- $ops$  interaction<sup>23,32</sup> or if the KOW domain might also participate, as proposed for Loaf<sup>55</sup>. Attempts to purify a Class-1 NGN alone yielded only insoluble protein. Instead, we compared NGN-KOW  $Y_E$ - $Y_B$  hybrids to  $Y_E$  and  $Y_B$  on  $ops_E$ ,  $ops_B$ , and an  $ops_{E-B}$  hybrid scaffold (Fig. 5f). For both  $Y_E$  and  $Y_B$ , the effect on capture or pausing was determined completely by the NGN domains. We conclude that recognition of  $ops_X$  by at least Class-1  $Y_X$  is mediated by the NGN and not the KOW domain.

### **Class-1 $Y_X$ protects upstream DNA from exonucleolytic cleavage**

For the  $Y_X$  NGN to contact upstream duplex DNA, the DNA must distort from a canonical B-form trajectory departing the PEC (Fig. 6a). Although protein interactions can easily bend duplex DNA<sup>60</sup>, we sought direct physical evidence for usDNA- $Y_X$ -NGN interaction. Exonuclease III (ExoIII) has been used extensively to detect PEC boundaries on DNA<sup>61–63</sup>. Since  $Y_{E,B}$  variably depend on distal usDNA in our activity assays, we assayed  $ops_{E,B}$  with cognate  $Y_X$ .

Over the full time course,  $Y_{E,B}$  strongly stabilized a -21 footprint, 6–7 base pairs upstream of RNAP (Supplementary Fig. 12). However,  $Y_B$  but not  $Y_E$  also slowed ExoIII digestion at -24, and -31 to -34. Further, these same upstream protections were caused by a  $Y_{B,E}$  NGN-KOW hybrid (Fig. 6b and Supplementary Fig. 12). We conclude that  $Y_B$  NGN likely contacts usDNA at least near -21 to -24, and -31 to -34.

As an additional test of the upstream  $Y_B$  contacts, we performed ExoIII assays on scaffolds containing  $ops_B$ -to- $ops_E$  sequence changes to distal usDNA (-36 to -34 and -26 to -24) and proximal usDNA (-18 to -16). These substitutions strongly reduced upstream protection from ExoIII (Fig. 6c and Supplementary Fig. 13). Together, our results suggest a set of  $Y_X$  specificity determinants reflected in both physical contacts detected with ExoIII and sequence effects on  $Y_X$  activity.

To understand these contacts in a structural context, we modeled  $Y_E$  and  $Y_B$  into an RfaH- $ops$ -PEC structure (PDB 8PHK)<sup>33</sup>. Both  $Y_E$  and  $Y_B$  are predicted to have a much larger positively charged surface approximately in the path of the usDNA (Supplementary Fig. 14). This charge is created largely by basic residues in the beta hairpin mini-

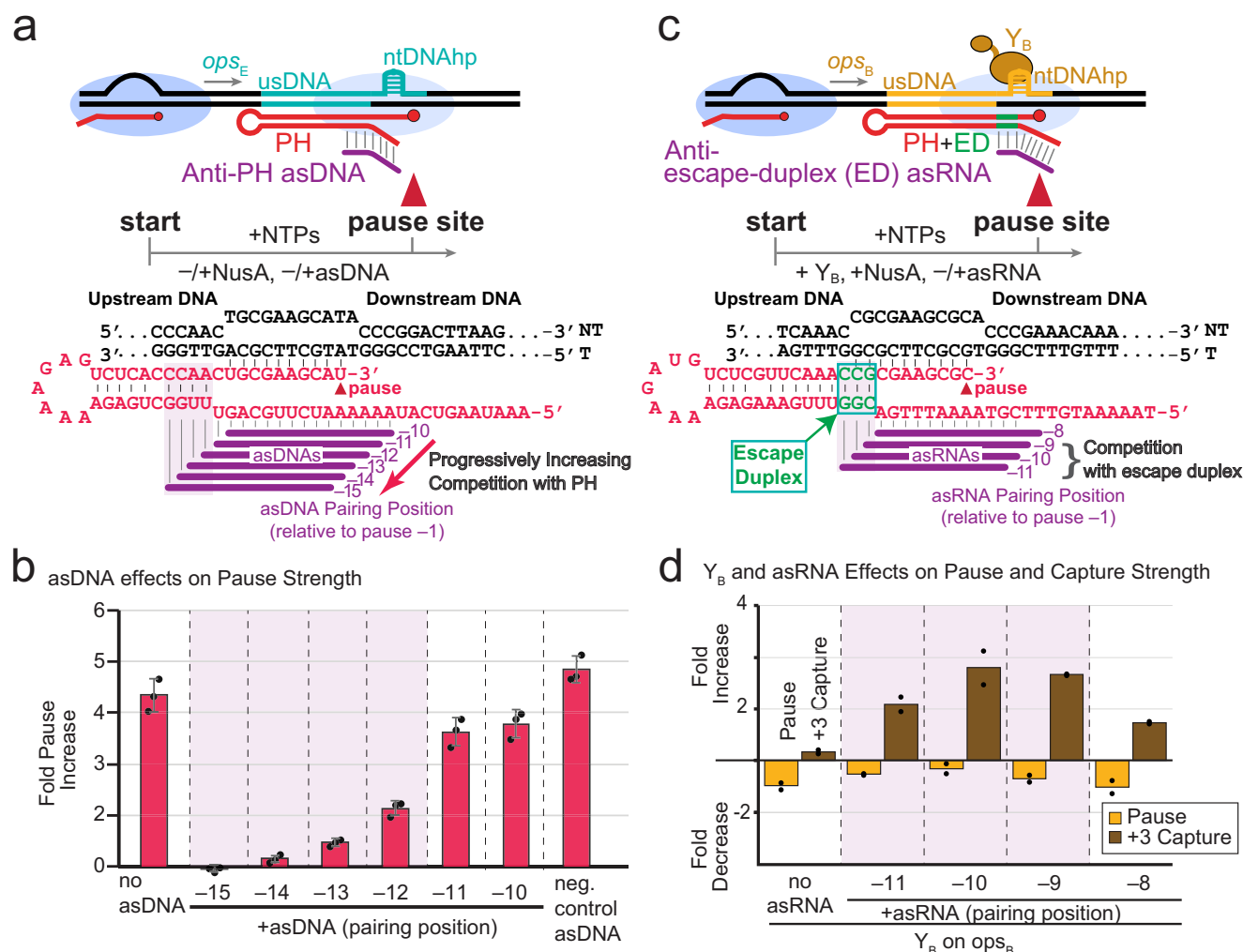


**Fig. 4 | Nascent RNA hairpins promote pausing or pausing-then-escape at *ops<sub>X</sub>*.**

**a** Experimental scheme. *rBfr*RNA was reconstituted upstream of the *ops<sub>E</sub>* pause, enabling PH formation upon RNA extension. **b** Antisense DNA (asDNA; 10  $\mu$ M final) effects on NusA enhancement of PH-stimulated *ops<sub>E</sub>* pausing, where different asDNAs disrupt PH formation to different extents. asDNA oligonucleotides were added concomitantly with NusA (or storage buffer) and NTPs (1  $\mu$ M and 100  $\mu$ M each NTP, final). Data are presented as mean values  $\pm$  SD from  $n = 3$  independent experiments. **c** Experimental scheme. *rBfr*RNA was reconstituted upstream of *ops<sub>B</sub>*

pause, enabling PH formation. **d** Antisense RNAs (asRNAs; 0.5  $\mu$ M final) pairing with an escape duplex (ED, green; the ED is unique to PSA and PSB). asRNAs inhibited PEC escape, leading to accumulation of a captured RNA (*ops<sub>B</sub>* + 3 nt). Assays were performed in the presence of 1  $\mu$ M NusA and 150 nM  $Y_B$ . The amount of RNA paused or captured 45 s after addition of NTPs is shown. Fold changes are relative to plus NusA and minus  $Y_B$ . Data are presented as mean values with data points from  $n = 2$  independent experiments shown.

domain of  $Y_{E,B}$  and could position the usDNA for sequence-specific readout by NGN.

## Discussion

Human gut *Bacteroides* strains synthesize numerous surface CPS that are highly regulated to create subpopulations in which primarily a single PS locus is transcribed, providing phenotypic plasticity to environmental challenges. To coordinate CPS gene expression in a manner that maximizes CPS diversity, *Bacteroides* have developed a complex hierarchy involving locus-specific cognate  $Y_X$  activation and noncognate  $Z_X$  inhibition.

We have elucidated the biochemical mechanisms of *Bacteroides* CPS hierarchical control (Fig. 7): (i) *Bfr*RNA pauses prominently at single CPS leader-region pause sites (*ops<sub>X</sub>*); (ii) *ops<sub>X</sub>* programs NusA-enhanced, RNA hairpin-stabilized transcriptional pauses that create time windows for  $Y_X$  recruitment; (iii)  $Z_X$  inhibits non-cognate  $Y_X$  directly via differential binding affinities, forming a heterodimer that precludes  $Y_X$  recruitment by steric clash of  $Z_X$  with RNAP and *ops<sub>X</sub>*; (iv)  $Y_X$  locus-specific recruitment depends on multipartite interactions of

the  $Y_X$  NGN domain with the exposed *ops<sub>X</sub>* ntDNA and upstream duplex DNA; (v)  $Y_X$ s evolved into functionally distinct classes; and (vi)  $Y_X$ -bound PECs use different mechanisms to escape *ops<sub>X</sub>*. This combination of multiple functions at a single RNAP pause site has little precedent and may reflect the strong evolutionary pressure associated with the challenges of discriminating among multiple similar NusG<sub>SP</sub>s.

*Bacteroides* belong to the greater phylum Bacteroidota, evolutionarily distant from the commonly studied model proteobacterium *E. coli* and firmicute *B. subtilis*. Despite the importance of these bacteria to human health, there is a limited understanding of *Bacteroides* transcription regulation. Our recombinant *Bfr*RNA overexpression system enables facile production and genetic manipulation of *Bfr*RNA. Multiple questions can now be addressed, including the roles of uncharacterized RNAP sequence insertions<sup>64</sup>, the molecular interactions of RNAP with TFs (e.g.,  $\sigma^A$ ) and small molecules (e.g., ppGpp), and sequence-dependent effects on transcriptional activities (e.g., backtracking, translocation, etc.). Recombinant RNAPs enable studies of both lineage-specific transcription mechanisms and evolutionary comparisons. *rBfr*RNA will enhance mechanistic understanding in the

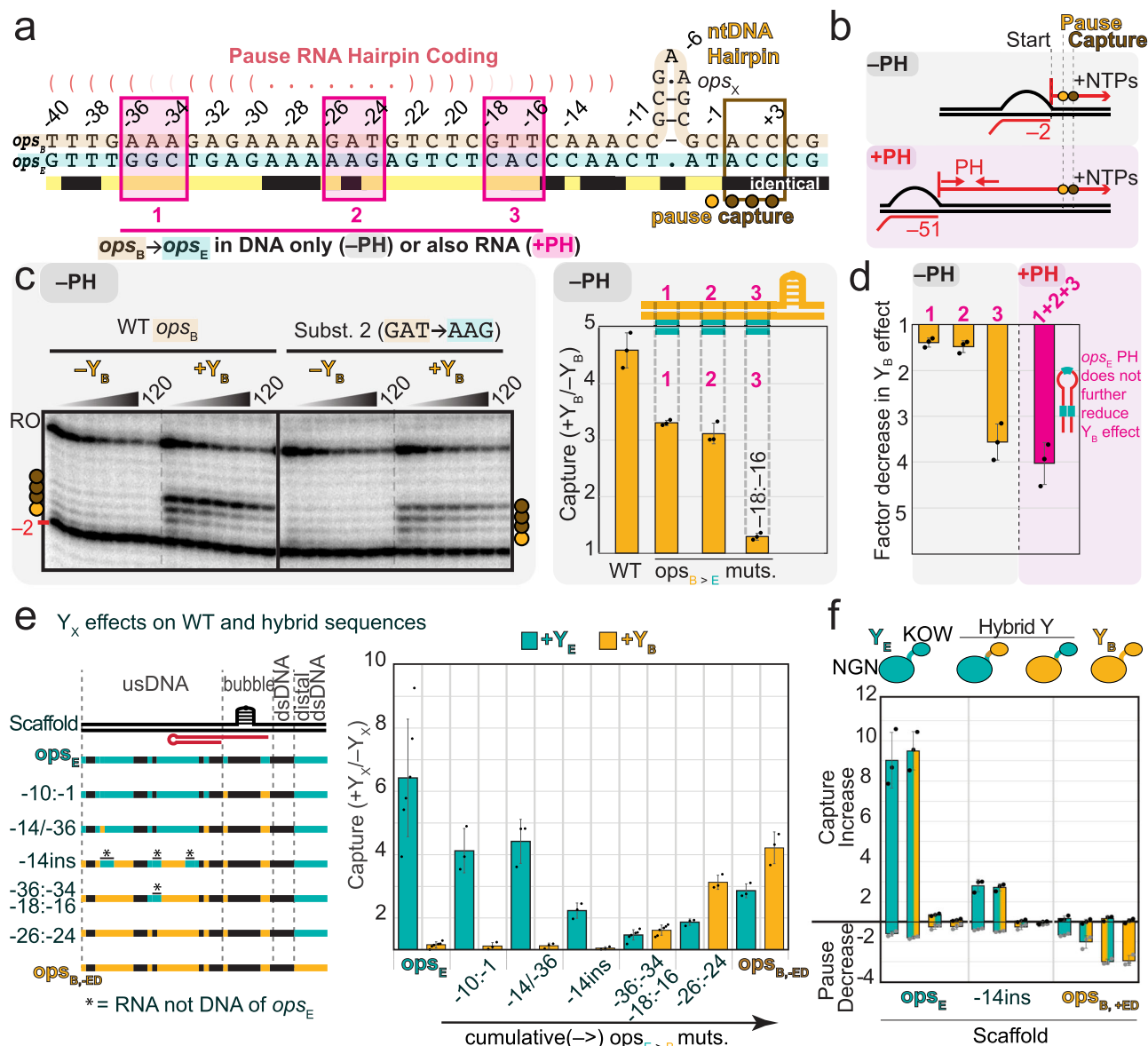


**Fig. 5 | Y<sub>X</sub> distinguish ops<sub>X</sub> binding sites through variations in the non-template DNA and upstream duplex DNA. a** Diagram comparing Class 1 ops<sub>E</sub> and ops<sub>B</sub> sequences. Regions varied in experiments shown in (b–d) are highlighted in magenta. **b** Experimental scheme to assay effects of the usDNA and PH. **c** PIVOT assays (1 μM NusA, 100 μM each NTP, 150 nM Y<sub>X</sub> when added) comparing Y<sub>B</sub> fold effects on capture on WT versus mutant scaffolds. Y<sub>B</sub> causes capture in these experiments because native RNA structures are not permitted to form (including the escape duplex (ED)). The gel panel depicts time-courses of pausing on WT ops<sub>B</sub> vs a mutant having substitution 2 from (a). Right: results from a representative single time-point (i.e., 10 s after NTP addition) comparison of Y<sub>B</sub> effects across multiple mutant scaffolds. Data are presented as mean values ± SD from *n* = 3

independent experiments. **d** Comparison of Y<sub>B</sub> effects in the absence or presence of a PH (the ops<sub>B</sub> scaffold plus PH was designed to prohibit ED formation to enable this comparison). Data are presented as mean values ± SD from *n* = 3 independent experiments. **e** Y<sub>X</sub> fold effect on pausing at the 45 s time point on WT ops<sub>E</sub> or hybrid sequences progressively mutated from ops<sub>E</sub> towards ops<sub>B</sub> with the ED disrupted (see Supplementary Fig. 11 for scaffold sequence). PIVOT assays were performed at a single timepoint (45 s). Data are presented as mean values ± SD from *n* = 3 or *n* = 6 independent experiments. **f** PIVOT assay of pause and capture for WT vs Hybrid NGN-KOW Y<sub>X</sub> (150 nM each) on WT vs hybrid (labeled ‘-14ins’) ops<sub>X</sub> sequences. Data are presented as mean values ± SD from *n* = 3 independent experiments.

entire field of transcription, as demonstrated by numerous recent studies in *M. tuberculosis*, *C. difficile*, and *B. subtilis*<sup>26–28,65,66</sup>.

We found that ops<sub>X</sub> recruitment sites for Y<sub>X</sub> are -40 bp multipartite DNA elements with both upstream duplex and transcription bubble ntDNA components, in striking contrast to the 12-nucleotide ntDNAhp (ops) necessary for RfaH-recruitment and the proposed nascent RNA hairpin necessary for Loap recruitment<sup>32,55</sup>. The ntDNAhps formed by ops and ops<sub>X</sub> differ in apparent structure and position relative to the pause site. All eight ops sites in *E. coli* targeted by the single RfaH encode the same ntDNAhp sequence: 5'-GCCGTAGC<sup>67</sup>. The longer *Bacteroides* 5'-YCGGNAGCR ntDNAhps

exhibit both similar (GCG..AGC stems) and distinct (loop) features compared to ops. These differences highlight how *Bacteroides* evolved to manage numerous NusG<sub>sp</sub>. Extensive Y<sub>X</sub>-ops<sub>X</sub> interactions may also accelerate *Bacteroides* adaptation by expanding the sequence space available for functional bifurcation following gene duplication.

We found that Z<sub>X</sub> inhibits Y<sub>X</sub> recruitment to ops<sub>X</sub>-PECs directly, likely by blocking Y<sub>X</sub> interaction with the conserved β' clamp helices (CH) and the ops<sub>X</sub> usDNA. Z<sub>X</sub> could also tune heterologous operon PSX expression or limit self-expression through negative feedback. Ultimately, Y<sub>X</sub>-Z<sub>X</sub> interactions define the cell surface architecture of



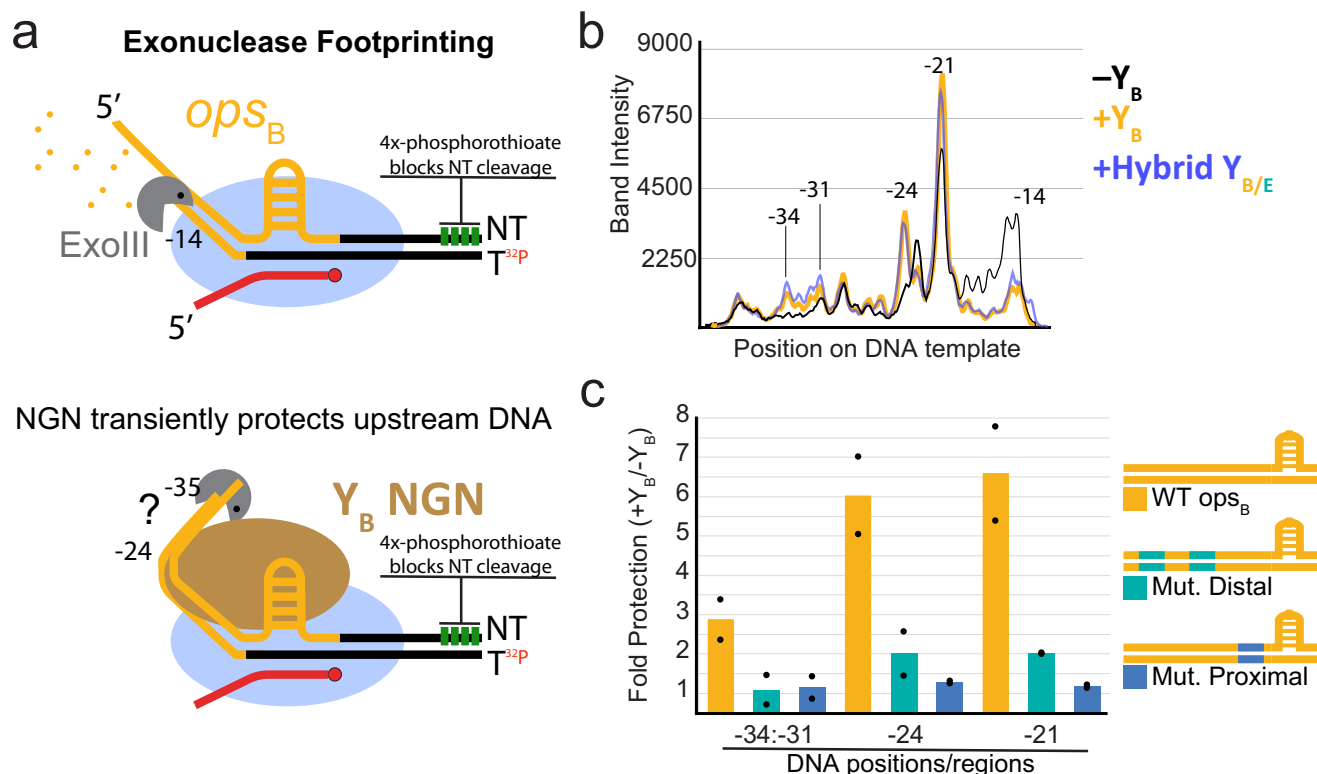


**Fig. 6 |  $Y_X$  contacts sequences in the upstream duplex DNA and ntDNAhp to recognize cognate  $ops_X$  via a capture-then-escape mechanism. **a**  $Y_X$  protects the distal upstream DNA from exonucleolytic cleavage. Exonuclease III (ExoIII) cleaves in the 3'-to-5' direction but temporarily halts when encountering obstacles such as DNA-bound proteins. Protection was assayed in the absence or presence of  $Y_X$  or hybrid NGN-KOW at various timepoints. **b** Pseudodensitometry traces of template**

DNA cleavage products separated by 8% Urea-PAGE. Band intensities reflect relative levels of cleavage products after 5 s of exonucleolytic cleavage. Traces are representative of experiments performed in at least duplicate (Supplementary Fig. 12). **c** Quantification of upstream DNA protection from exonucleolytic cleavage at various regions on WT or mutant  $ops_B$  scaffolds. Data are presented as mean values with data points from  $n = 2$  independent experiments shown.

*Bacteroides*. Our findings provide a foundation for understanding them.

The closer Class-2 start-codon proximity to  $ops_X$  (9 bp) suggests that Class-2  $Y_X$  may play a stronger role in ribosome association for coupled transcription-translation of the  $Y_X$  gene. Translation is not well studied in *Bacteroides*<sup>68–71</sup>, but both the similarity of anti-pausing by *Bfr*NusG to *Eco*NusG (Supplementary Fig. 5) and the location of stop codons relative to intrinsic terminators<sup>72</sup> suggests transcription and translation may be coupled in *Bacteroides* – like *E. coli* but unlike *B. subtilis*<sup>72–82</sup>. RfaH is thought to recruit ribosomes for coupled translation in *E. coli*<sup>83,84</sup>. Start codon GUG is thought to initiate ribosomes 5–10 times more weakly than AUG in *E. coli*<sup>85</sup>. Taken together, these differences are consistent with evolution of Class-2  $Y_X$ - $ops_X$  pairs for tight linkage of  $Y_X$  and ribosome recruitment at  $ops_X$  sites immediately adjacent to the translation start site. Both these potential distinctions (relative to Class 1) in Class-2  $Y_X$ - $ops_X$  function and interesting differences evident for  $Y_C$ - $ops_C$  and  $Y_G$ - $ops_G$  require future experimental investigation.

We also discovered a regulatory RNA element—the  $ops_X$  PH ED—involved in the regulation of PSA and PSB. The conserved role of PHs at  $ops_X$  is to enhance pausing with NusA. The  $ops_{A,B}$  ED provides a driving force to propel RNAP out of pause-cycling traps created by extensive interactions that occur at these sites. Possibly,  $ops_E$  does not encode an ED because  $Y_E$  interacts with less sequence (Supplementary Fig. 12) and Gre factor may be sufficient for its escape as it is for RfaH<sup>33</sup>. Alternatively, the strong kinetic difference in escape mechanisms could be exploited by *Bacteroides* in CPS expression control. We propose that the ED evolved in response to evolutionary pressure to expand  $Y_X$  specificity.

Our results provide new mechanistic insights into transcriptional regulation by a large class of NusG<sub>SP</sub>,  $Y_X$  (Up $x$ Y). We find that determinants of transcriptional pausing in the phylum Bacteroidota resemble those found for other bacteria, but that recruitment sites for these NusG<sub>SP</sub>s differ notably both in being multipartite and much more extensive (~40 bp) than found for *E. coli* RfaH (~12 bp). Two aspects of the  $Y_X$  recruitment mechanisms provide precedent for new types of transcriptional regulation: (1) the upstream DNA is a sequence-specific platform for PEC regulation, and (2) pause hairpins can include escape duplexes that can drive escape from regulator-stabilized pauses. These discoveries highlight the importance of studying transcriptional mechanisms in diverse bacteria.

## Methods

Plasmids, oligonucleotides, and strains used in this study are listed in Supplementary Tables S1–4. Nucleic acid scaffolds used in PIVoT assays are organized by figure in Supplementary Fig. 16. All reported measurements were taken from distinct samples.

### *E. coli* strain construction

*E. coli* strain RL3569 was created by P1 transduction of RL1674 with donor strain RL3570<sup>86</sup> harboring the rifampicin-resistance mutation S522F in *rpoB*. Briefly, 5 mL of donor strain RL3570 was grown to saturation (overnight) in LB + 5 mM CaCl<sub>2</sub>. The next day, 50  $\mu$ L of the donor strain was mixed with 100  $\mu$ L of a 10<sup>-5</sup> dilution (in LB + 5 mM CaCl<sub>2</sub>) of a freshly made P1 stock, then incubated at 37 °C for 20 min without shaking. 2.5 mL of 45c-equilibrated R top agar (0.8 % agar, 1% tryptone, 0.8% NaCl, 0.1% yeast extract, supplementing to a final concentration of 2 mM CaCl<sub>2</sub> and 0.1% glucose after autoclaving) was

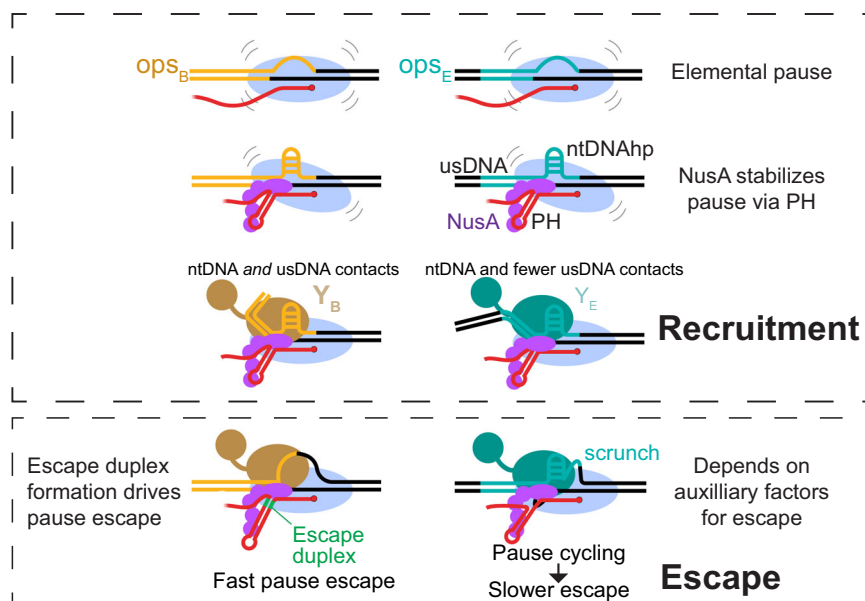


**Fig. 7 | Model for  $Y_x$ -specific recruitment.**  $BfrNAP$  pauses in the 5' leader of CPS operons to provide time for  $Y_x$  recruitment. These pauses arise initially through RNA–DNA contacts to RNAP (elemental pause), then are stabilized synergistically by a PH and NusA.  $Y_x$  is recruited with high fidelity to cognate operons by multipartite ~40-bp  $ops_x$  elements, with variable influence of constituent elements depending on

the CPS operon.  $Y_x$ s that interact extensively with cognate  $ops_x$  ( $Y_A$ ,  $Y_B$ ) are associated with escape duplex (ED)-encoding PHs, which provides force in the form of base-pairing to drive forward translocation and inhibit backtracking. Differences among escape mechanisms (e.g., those with or without EDs) may aid differential regulation.

added to the bacteria-phage mixture, flicked to mix, then poured evenly onto a thick, moist, freshly-made R plate (1.2% agar, 1% tryptone, 0.8% NaCl, and 0.1% yeast extract, supplementing to a final concentration 2 mM  $CaCl_2$  and 0.2% glucose after autoclaving). The plates were incubated at 37 °C overnight in a plastic bag with wet paper towels. The next day, the plate was transferred to a 4c room and overlaid with 5 mL of MC solution (10 mM  $MgSO_4$  + 5 mM  $CaCl_2$ ). After a 5 h incubation at 4 °C, the overlaid solution containing fresh P1 lysate was collected, 0.2  $\mu$ m filter-sterilized, then stored in the dark at 4c until use. The recipient strain (RL1674) was grown to saturation (overnight) in LB + 5 mM  $CaCl_2$  + 20  $\mu$ g chloramphenicol/mL. The next day, 100  $\mu$ L of donor P1 phage serial dilutions were separately mixed with 100  $\mu$ L of recipient strain overnight culture, then incubated at 37 °C for twenty minutes with no shaking. The mixture was plated on LB agar + 20  $\mu$ g chloramphenicol/mL + 100  $\mu$ g rifampicin/mL. Candidates were sequence-verified.

### *B. fragilis* strain construction

**Bacterial growth.** *B. fragilis* NCTC 9343 (ATCC25285; Genbank assembly ASM2598v1) strains were grown in basal medium<sup>87</sup> or on BHI plates supplemented with 5 mg hemin/liter and 2.5  $\mu$ g vitamin  $K_1$ /L. Mutants  $\Delta mpiM44$ <sup>17</sup>,  $\Delta mpiM44\Delta upaZ$ <sup>43</sup> and  $\Omega PSE$ <sup>41</sup> were previously constructed. For selection of cointegrants, gentamycin (200  $\mu$ g/mL) and erythromycin (5  $\mu$ g/mL) were added to the plates when indicated.

**Construction of mutant PSE  $ops$  and HP- $ops$  regions in 9343 $\Delta mpiM44$ .** Two different alterations to the PSE 5' UTR were made in the  $\Delta mpiM44$  strain. In the first mutant, the  $ops$  sequence of the PSE locus (CTGCGAAGCATA) was replaced with the  $ops$  sequence of the PSA locus (cgcgtagcgca). In the second mutant, a larger replacement was made and included the hairpin region adjacent to the  $ops$  sequence. The sequence from the PSE 5' UTR (ttggctgagaaaaagagctcaccacaaCTGCGAAGCATA) was replaced with the sequence from the PSA 5'UTR (cggtttgatgggaaaagatgtctcgtccaaaccgtagcgca). The recombinant plasmids were created by PCR amplifying two ( $ops$ ) or three (HP- $ops$ ) DNA segments using Phusion polymerase (NEB) with  $\Delta mpiM44$  as template with the primers listed in Table S2. These

segments were cloned into BamHI-digested pLGB13<sup>88</sup> using NEBuilder (NEB). Plasmids were sequenced to confirm the correct assembly of the segments. Plasmids were conjugally transferred from *E. coli* S17  $\lambda$ pir to  $\Delta mpiM44$  and after overnight co-incubation, were plated on BHIS with gentamycin and erythromycin. The resulting cointegrants were passaged in basal medium for several hours and plated on BHIS with 50 ng anhydrotetracycline to select for double cross-over recombinants. These strains were tested by PCR for replacement of the PSE sequences with the respective PSA sequences and the genomes of these two strains were sequenced to confirm the correct replacements.

### Western immunoblot analysis

Bacterial strains were grown overnight to an apparent  $OD_{600}$  of ~1.2. Bacteria were pelleted and resuspended in 1 $\times$  LDS loading buffer (Invitrogen) and boiled for 5 min. Cell lysates (equivalent to 3.5  $\mu$ L of the original culture) were loaded onto 4–12% NuPAGE (Invitrogen) and run with MES buffer until the 17 kDa molecular weight standard had run to the bottom of the gel to allow for migration of the high molecular weight PSE further into the gel. The contents of the gel were transferred to PVDF and blocked with 5% skim milk in TBS with 0.5% tween (TBST). The blot was probed with a mouse monoclonal antibody specific to PSE (Supplementary Fig. 15) used at 1:100 dilution, washed with TBST, and probed with a 1:2000 dilution of alkaline phosphatase conjugated goat-anti rabbit IgG (Invitrogen Catalog # 31340 Lot YA366475). After washing with TBST, the blot was developed with BCIP/NBT (KPL).

### NET-seq

*B. fragilis* NCTC 9343 rpoC-3xFLAG was streaked onto BHIS plates and incubated at 37 °C anaerobically for 2 days. A swab from a dense area on the plate was used to inoculate overnight cultures. The next day, 10 mL of the overnight culture was used to inoculate 500 mL SBM (starting apparent  $OD_{600}$  0.04 as measured by a Denville® CO8000 Personal Cell Density Meter). When the apparent  $OD_{600}$  measured 0.65, cultures were removed from the anaerobic chamber and 300 mL was used for subsequent steps.

To harvest nascent transcripts for the NET-seq workflow, cultures were filtered between two vacuum filtration systems using a 0.45 µm pore nitrocellulose filter (GVS Micron Sep, 1215305). Cells were scraped off each filter using a spatula and plunged immediately into liquid nitrogen (i.e., cells from the same culture were combined into the same 50 mL conical tube containing ~25 mL liquid nitrogen). Collected cells were cryo-lysed using a RETSCH mixer mill (MM 400) as previously described<sup>37</sup>, with the exception that 50 mL stainless steel canisters and a 25 mm stainless steel ball were used to perform the cryomilling.

To isolate nascent transcripts, we performed a modified 3xFLAG-IP protocol with previously described buffers<sup>37</sup>. Specifically, the thawed grindate volume was scaled to 5.5 mL with lysis buffer (1× lysis stock [20 mM Tris, pH 8.0, 0.4% Triton X-100, and 0.1% NP-40 substitute], 100 mM NH<sub>4</sub>Cl, 1× EDTA-free cOmplete Mini protease inhibitor cocktail [Roche Diagnostics GmbH, 11836170001], 10 mM MnCl<sub>2</sub>, and 50 µM RNasin [Promega, N211B], and 0.4 mg/mL puromycin), DNA was partially digested for 20 min with RQ1 DNase (0.054 µM [0.02 µM for the *E. coli*-only NET-seq pilot experiment]) [Promega, M6101], and digestion reactions were stopped by addition of EDTA to 28 mM (final concentration). RNAP-nascent transcript complexes were directly immunoprecipitated using Anti-FLAG M2 affinity gel (Sigma, A2220) (i.e., without buffer exchange), and the precipitated RNAP-nascent transcript complexes were subsequently washed four times (1× lysis stock, 100 mM NH<sub>4</sub>Cl, 300 mM KCl, 1 mM EDTA, and 50 µM RNasin) [Promega, N2515]. RNAP-nascent transcript complexes were eluted twice with 3xFLAG peptide (Sigma, F4799) (1× lysis stock, 100 mM NH<sub>4</sub>Cl, 2 mg/mL 3xFLAG peptide, 1 mM EDTA, and 50 µM RNasin). Nascent transcripts were purified using a miRNeasy kit [Qiagen, 217084] as previously described<sup>37</sup>. However, to reduce phenol and chaotropic salt contamination, nascent transcripts were subjected to an additional overnight isopropanol-GlycoBlue (Invitrogen, AM9516) precipitation at −20 °C.

For nascent transcript library generation, we followed a modification of a previous NET-seq workflow<sup>36,37</sup>. Specifically, our workflow included using custom adaptors compatible with an Illumina NovaSeq X instrument. Likewise, the DNA adapter used for nascent transcript 3' end ligation was adenylated using components from a NEB 5' DNA Adenylation kit (E2610; 6 µM DNA linker [RL15032], 80 µM ATP, 6 µM Mth RNA ligase, and 1× Adenylation Reaction Buffer). The adenylation reaction was incubated for 4 h incubation at 65 °C, inactivated at 85 °C for 5 min, and precipitated overnight at −20 °C with isopropanol and GlycoBlue (Invitrogen AM9516). The precipitated, adenylated DNA linker was ligated to 750 ng of precipitated nascent transcripts, in duplicate, using components of a NEB T4 RNA Ligase 2, truncated (T4 Rnl2tr) kit (M0242; 10% DMSO, 22% PEG8000, 3 µM adenylated DNA linker, T4 Rnl2tr [14.7 µM], RNasin [2 µM], and 1× T4 RNA Ligase Reaction Buffer). These ligation reactions were incubated at 37 °C for 4 h. After this incubation, T4 Rnl2tr was inactivated by incubation with Proteinase K (0.04 µM) (NEB, P8107) at 37 °C for 1 h. RNAs were fragmented, resolved, gel extracted, and precipitated as previously described<sup>36,37</sup>, with the exception that the gel extraction incubation at 70 °C was increased to 25 min. cDNAs were synthesized using a custom adapter (RL14637) and a previously described protocol<sup>36,37</sup>, with the exception that the reaction time was increased to 1 h. Circularization of gel extracted and precipitated cDNAs was performed using a protocol previously described<sup>36,37</sup>, with the exception that the circularization reaction incubation period was increased to 3 h and the gel extraction incubation period was increased as above. After circularization, cDNA libraries were PCR amplified using minimal cycles and custom adaptors, gel extracted, and precipitated as previously described<sup>36,37</sup>. Library concentration and amplified product size distribution were determined using an Agilent TapeStation 4150. NET-seq libraries were sequenced by the University of Wisconsin-Madison Biotechnology Center on an Illumina NovaSeq X instrument. NET-seq data were

processed using a combination of custom scripts and standard tools. Briefly, adapters, linker, and control oligos potentially contaminating each sample were trimmed from raw reads using cutadapt (v3.4). Reads with a minimum length of 14 nts were mapped to the *B. fragilis* genome (NC\_003228.3) using Bowtie (v1.3.0) allowing both one mismatch and random assignment of reads mapping to multiple loci based on alignment stratum (Bowtie options `-best -a -M 1 -v 1`). Alignments were converted to BAM and BED files using samtools (v1.16.1) and bedtools (v2.30.0). The specific 3' end counts for each genome position were determined using bedtools (options `-d -strand -5 [plus strand] or -d -strand + -5 [minus strand]`).

### ***rBfr* RNAP cloning and purification**

*B. fragilis* RNAP coding regions were codon-optimized using Gene Designer from DNA2.0 (now ATUM) using *E. coli* codon frequencies<sup>89</sup> and amplified from synthetic DNA (IDT) of *B. fragilis* NCTC 9343, then cloned into a pRM756 backbone<sup>90</sup>, incorporating a His10-ppx tag at the C-terminus of β' and a Strep tag at the N-terminus of β. RBS sites were optimized using denovodna.com<sup>91,92</sup>. This plasmid enables T7 overexpression of all subunits under IPTG control.

*rBfr* RNAP was purified similarly to *E. coli* RNAP<sup>93</sup>, with changes described below. Following transformation of RL3569 with pJS015, a colony was picked and inoculated into a 3 mL LB + 25 µg kanamycin/mL + 20 µg chloramphenicol/mL. Two milliliter of overnight culture was used to inoculate 2 L LB + 25 µg kanamycin/mL + 10 drops Sigma Antifoam Y-30 Emulsion in baffled Fernbach flasks and incubated at 37 °C. When the apparent OD<sub>600</sub> reached 0.4, the temperature was dropped to 16 °C, overexpression was induced by addition of 200 µM IPTG, and incubation was continued with shaking at 200 RPM overnight (~18 h). Cell cultures were placed on ice for 20 min, then pelleted by centrifugation at 3000 × *g* for 15 min at 4 °C.

Moving forward, all steps were performed at 4 °C or on ice, and all buffers were filtered through 0.2 µm filters. Pellets were resuspended in 30 mL lysis buffer (50 mM Tris-HCl pH 8.0, 5% glycerol, 100 mM NaCl, 2 mM EDTA, 10 mM BME, 10 mM DTT, 0.1 mg/mL phenylmethylsulfonyl fluoride, with one dissolved tablet of Roche cOmplete™ ULTRA EDTA-Free Protease Inhibitor Cocktail). The resuspended cell solution was sonicated for 20 min total (alternating sonication on/off times of 5 min) with settings Power 8, Duty Cycle 20%. The lysate was then transferred to round-bottom polycarbonate tubes and spun at 27,000 × *g* for 15 min. The supernatant was transferred to a 100 mL beaker with stir bar, then 6.5% PEI was slowly added to a final concentration of 0.6% while stirring. The solution was stirred for one hour, then transferred to open-top, round-bottom polycarbonate tubes and spun at 11,000 × *g* for 15 min. After decanting supernatant, a tissue homogenizer was used to resuspend the pellet in 25 mL of TGEDZ (10 mM Tris-HCl pH 8.0, 5% glycerol, 0.1 mM EDTA, 5 µM ZnCl<sub>2</sub>, 1 mM dithiothreitol) with added 0.3 M NaCl. The solution was spun at 11,000 × *g* for 15 min. After decanting supernatant, a tissue homogenizer was used to resuspend the pellet in 25 mL of TGEDZ with added 1 M NaCl. The solution was spun at 11,000 × *g* for 15 min. The supernatant was transferred into a 100 mL beaker with stir bar, then finely-ground AmSO<sub>4</sub> was added to the stirring solution to a final concentration of ~0.37 g/mL and precipitated overnight. The solution was transferred to Oak Ridge round-bottom tubes and spun at 27,000 × *g* for 15 min.

The pellet was dissolved in 35 mL of HisTrap Binding Buffer (20 mM Tris-HCl pH 8.0, 500 mM NaCl, 5 mM imidazole, 5 mM beta-mercaptoethanol (BME), then spun at 27,000 × *g* for 15 min in the same Oak Ridge round-bottom tube. The supernatant was filtered through 0.2 µm filters and applied at 1 mL/min to a HisTrap HP 5 mL column, pre-equilibrated with HisTrap Binding Buffer. The column was washed with HisTrap Binding Buffer at 5 mL/min until A280 reached baseline, then washed at 5 mL/min with 2% HisTrap Elution Buffer (20 mM Tris-HCl pH 8.0, 500 mM NaCl, 1 M imidazole, 5 mM beta-mercaptoethanol



[BME]) until A<sub>280</sub> reached baseline. rBfrNAP was eluted at 5 mL/min with a 2–50% gradient of HisTrap Elution Buffer (translating to a 20–500 mM imidazole gradient). Three milliliter elution fractions containing rBfrNAP were pooled, filtered through 0.2 µm filters, then the NaCl concentration was reduced to 150 mM for the following purification step by dilution with TGEDZ buffer.

HisTrap elution fractions were pooled then diluted with 100 mM Tris-HCl, pH 8.0, 1 mM EDTA, 10 mM DTT to adjust the salt concentration to 150 mM NaCl. The sample was then applied to a 5 mL Strep-Tactin® XT High Capacity column pre-equilibrated with 2 CV Buffer W (100 mM Tris-HCl, pH 8.0, 150 mM NaCl, 1 mM EDTA, 10 mM DTT) at 2 mL/min. The flow-through was reapplied to the column at 0.037 mL/min. The column was then washed with 5 CV of Buffer W. rBfrNAP was eluted with Buffer BXT (100 mM Tris-HCl, pH 8.0, 150 mM NaCl, 1 mM EDTA, 10 mM DTT, 50 mM D-Biotin (Acros Organics)).

Pooled fractions from the previous step were applied at 1.5 mL/min to a HiTrap HP column pre-equilibrated with TGEDZ + 200 mM NaCl. The column was then washed with TGEDZ + 200 mM NaCl until A<sub>280</sub> reached baseline, then rBfrNAP was eluted with TGEDZ + 500 mM NaCl at 2.5 mL/min.

Pooled fractions from the previous step were dialyzed overnight in RNAP storage buffer (10 mM Tris-HCl, pH 8.0, 25% glycerol, 100 mM NaCl, 100 µM EDTA, 1 mM MgCl<sub>2</sub>, 20 µM ZnCl<sub>2</sub>, 10 mM DTT) using a 10 kDa MWCO cassette, then concentrated using Ultra-4, MWCO 100 kDa (Sigma-Aldrich Z648043-24EA) to a final concentration of 8 µM. The solution was then aliquoted, flash-frozen, and stored at –80 °C.

### Cloning and purification of transcription factors

All TFs (NusG, NusA, Y<sub>A</sub>, Y<sub>B</sub>, Y<sub>C</sub>, Y<sub>E</sub>, Y<sub>F</sub>, Y<sub>H</sub>, Y<sub>B</sub>(NGN)–Y<sub>B</sub>(KOW), Y<sub>E</sub>(NGN)–Y<sub>B</sub>(KOW)) were cloned into a pTYB2 backbone (Addgene catalog N6702S) after PCR amplification from *Bacteroides fragilis* ATCC 25285 (NCTC 9343) genomic DNA by NEB HiFi DNA assembly (Gibson Assembly). This vector enables IPTG-inducible over-expression of proteins fused at the C-terminus to the *Saccharomyces cerevisiae* VMA intein and chitin-binding domain. Importantly, to ensure efficient self-cleavage via the intein, an Ala residue was incorporated at the C-terminus of all transcription factor coding sequences.

After plasmid sequence verification, RL1674 (*E. coli* BL21 Rosetta™ (DE3)) was transformed by electroporation with pTYB2-derived constructs, then plated on LB agar with 100 µg ampicillin/mL and 20 µg chloramphenicol/mL (for retention of pRARE2 plasmid). For each expression construct, a single colony was picked and used to inoculate a 3 mL overnight LB culture grown at 37 °C containing the same concentration of antibiotics. The next day, 1 mL of overnight culture was used to inoculate a 200 mL LB culture containing antibiotics (3% ethanol was added for all Y<sub>X</sub> constructs) and grown at 37 °C. When the OD reached 0.2–0.3, the incubation temperature was dropped to 16 °C and shaking continued for 30 min. Subsequently, a final concentration of 200 µM IPTG was added and incubation continued overnight (16–18 h). The next day, cultures were placed on ice for 20 min, then pelleted at 3000 × g for 15 min at 4 °C.

Pellets were resuspended in 40 mL of Chitin Wash Buffer (CWB; 30 mM Tris-HCl, pH 7.5–8.0 depending on protein pI, 0.5 M NaCl, 1 mM EDTA, 0.05% Tween® 20) plus one dissolved tablet of Roche cOmplete™ ULTRA EDTA-Free Protease Inhibitor Cocktail. The cell suspension was sonicated 10 min at 20% duty cycle, Power 8. The lysate was pelleted at 30,000 × g for 30 min at 4 °C, then the supernatant was passed through 0.2 µm filters.

The subsequent steps were performed at room temperature closely following manufacturer's instructions. Briefly, 3 mL of a homogeneous suspension of NEB Chitin Resin (Catalog S6651L) were loaded into a 25 mL Poly-Prep Gravity Chromatography Column (Biorad), washed with 5 mL of mQH<sub>2</sub>O, then equilibrated by washing 3 times

each with 10 mL of CWB. The lysate was subsequently loaded onto the column, then washed three times each with 10 mL of CWB. Cleavage Buffer (CB) was made by adding 500 µL of 1 M DTT (prepared fresh from solid reagent) to 10 mL of CWB, then a quick flush was performed by adding 3 mL of CB. SDS-PAGE revealed no premature elution in the quick flush fraction. Immediately after dripping stopped, the bottom and top of the column were capped, parafilmed, and the column was incubated at room temperature overnight (16–18 h) to allow sufficient time for cleavage. The next day, cleaved protein was eluted by addition of 1.5 mL CWB + 10 mM DTT, then dialyzed overnight in 10 mM Tris-HCl, pH 7.5–8.0 depending on pI, 2% glycerol, 100 mM NaCl, 100 µM EDTA, 10 mM DTT using a 10 K MWCO cassette. After removal from the dialysis cassette, additional glycerol was added to a final concentration of 25%. The solution was aliquoted, flash-frozen, then stored at –80 °C until use.

### PIVoT assays

A direct reconstitution approach was used to assemble elongation complexes (ECs). Briefly, RNA and template DNA oligonucleotides were mixed at a ratio of 1:1.2 (5 µM: 6 µM) in transcription buffer (TB; 20 mM Tris-OAc, pH 7.7, 40 mM KOAc, 5 mM Mg(OAc)<sub>2</sub>, 1 mM DTT), then annealed by slow cooling in a thermocycler. To assemble 10× ECs, first the annealed RNA:tDNA scaffold and RNAP were mixed in TB and incubated for 15 min at 37 °C. Then, non-template DNA oligonucleotide was added and incubation continued for an additional 15 min at 37 °C. The solution was diluted with TB to prepare 2× EC (subtracting volume of further additions) and incubated for 1 min at 37 °C. Then, 5 µCi of [α-<sup>32</sup>P]NTP (depending on the scaffold) was added and incubated for 3 min at 37 °C. Additional GTP was added such that the final concentration of GTP in the solution was 10 µM, and incubation continued for 3 min at 37 °C.

2× ECs were aliquoted and all comparisons made were therefore performed with identically formed ECs. The assay was performed at 37 °C: transcription was restarted by addition of 2× NTPs minus/plus TFs or storage buffer. For Fig. 5c, Y<sub>B</sub> was pre-incubated with halted ECs following reconstitution at –3 and incorporation labeling to –2 prior to restarting transcription. Timepoints were taken by mixing 5 µL reaction aliquots with 5 µL of 2× Stop Buffer (25 mM EDTA, 8 M Urea, 1× TBE, 0.1% bromophenol blue, 0.1% xylene cyanol). The ratio and concentrations of EC components in the 1× EC solution was 1:1.2:1.4:1.6 (R:T:RNAP:NT; 50 nM, 60 nM, 70 nM, 80 nM). The final reaction concentrations of TFs are indicated in each figure legend. Unless otherwise indicated, NTPs are added to a final reaction concentration of 100 µM. RNAs were resolved by 8% or 15% Urea-PAGE with 0.5× TBE running buffer until the leading dye ran off the gel. Gels were exposed to PhosphorImager screens and scanned using a Typhoon PhosphorImager. To quantify effects in ImageQuant, boxes were drawn around the pause band *ops<sub>X</sub>*, the capture band(s) (if applicable), and beyond. After subtracting background, the fractions of RNA at *ops<sub>X</sub>* or at capture positions were averaged and errors reflect standard deviation from at least three replicates (unless indicated otherwise).

For the Z-titration assay in Fig. 2d, data were fit in Kaleidagraph to a sigmoidal function of the form  $y = a + (b-a) / (1 + (x/c)^d)$  where  $a = y_{min}$ ,  $b = y_{max}$ ,  $c$  is the Z<sub>X</sub> concentration at mid-point, and  $d$  is slope at mid-point; and weighted by standard deviation (error bars) from three assays.

### Biolayer interferometry

Preparation of biotinylated-Y<sub>E</sub>: pJS060 was cloned similarly to other pTYB2-derived constructs (see above), with the exception that two oligos were included in the Gibson assembly to introduce the 16 codon Avi-tag™ onto the N-terminus of upeY. Expression, cell harvesting, and lysis conditions are as described above. Avi-Y<sub>E</sub> was biotinylated on a gravity column as described below:



The subsequent steps were performed at room temperature closely following NEB instructions. Briefly, 3 mL of a homogenous suspension of NEB Chitin Resin (Catalog S6651L) were loaded into a 25 mL Poly-Prep Gravity Chromatography Column (Biorad), washed with 5 mL of mQH<sub>2</sub>O, then equilibrated by washing 3 times each with 10 mL of CWB. The lysate was subsequently loaded onto the column, then washed three times each with 10 mL of CWB. The column was then washed with three times each with Avi Chitin Wash Buffer (AviCWB = 10 mM Tris 8.0, 0.5 M KGlu, 0.1% Tween20). Components from Avidity BirA500 Kit were used in the subsequent biotinylation reaction: a biotinylating solution (500  $\mu$ L AviCWB, 70  $\mu$ L of BiomixA, 70  $\mu$ L Biomix B, 10  $\mu$ L of 1 mg/mL BirA) was added to the column and the reaction was allowed to continue for 2.5 h. The column was subsequently washed three times each with 10 mL of CWB. Cleavage Buffer (CB) was made by adding 500  $\mu$ L of 1 M DTT (prepared fresh from solid reagent) to 10 mL of CWB, then a quick flush was performed by adding 3 mL of CB. Immediately after dripping stopped, the bottom then the top of the column were capped, parafilm, and the column was incubated at room temperature overnight (16–18 h) to allow sufficient time for cleavage. The next day, cleaved protein was eluted by addition of 1.5 mL CWB + 10 mM DTT, then dialyzed overnight in 10 mM Tris-HCl pH 7.5, 2% glycerol, 100 mM NaCl, 100  $\mu$ M EDTA, 1 mM DTT using a 10 K MWCO cassette. After removal from the dialysis cassette, additional glycerol was added to a final concentration of 20%. The solution was aliquoted, flash-frozen, then stored at  $-80^{\circ}\text{C}$  until use. Importantly, Biotin- $Y_E$  retained activity in vitro.

For each titration, 1 mL of 0.3  $\mu$ M biotinylated- $Y_E$  was prepared in Octet Binding Buffer 4.1 (OBB4.1 = PBS + 400 mM NaCl + 0.01% Triton X-100 + 0.25% BSA).  $Z_A$  solution was prepared at 100 nM in OBB4.1 with twofold serial dilutions down to 1.56 nM.  $Z_E$  solution was prepared at 500 nM in OBB4.1 with serial dilutions down to 31.3 nM. Plates were prepared for binding assays: in plate 1200  $\mu$ L of OBB4.1 was placed in each well of column 1 containing a biosensor (up to 8 biosensors per experiment); plate 2 (containing ‘half-area’ wells permitting 100  $\mu$ L volumes) column 1 contained 100  $\mu$ L/well of OBB4.1, column 2 contained 100  $\mu$ L/well of 0.3  $\mu$ M biotinylated- $Y_E$ , and column 3 contained 100  $\mu$ L/well of  $Z_X$  serial dilutions or buffer (as a blank/reference) prepared above.

A basic kinetics assay was performed using standard acquisition rates at  $30^{\circ}\text{C}$  on a ForteBio Octet RED96 system. Octet® Streptavidin (SA) Biosensors were pre-equilibrated for 10 min at 30c. Step times: Baseline (Plate 2 Column 1 (P2C1)) = 60 sec; Loading (P2C2 = 320 sec (or until 2 nm loading density reached); Baseline (P2C1) = 60 sec; Association (P2C3) =  $\geq 300$  sec; Dissociation (P2C1) =  $\geq 300$  sec.

Data were processed using Octet Data Analysis Software. The reference biosensor curve (bio- $Y_E$  + buffer in place of  $Z_X$ ) was subtracted from all binding curves. Traces were subsequently aligned along the  $Y$  axis at pre-association baseline with interstep correction performed at the dissociation step. Noise Filtering (Savitsky-Golay-Filtering, smoothingfunction) was performed. Data from each experiment were independently globally fit. For each binding pair tested, two out of three global fits have  $R^2$  values around 0.95 or greater and chi-squared values less than 3 as recommended by ForteBio. Given the two orders of magnitude difference in binding constants, limited conclusions we are making, and parsimonious agreement of these constants among replicates and with our PIVO assays, we deemed the fits overall acceptable. The average and standard deviation of the kinetic parameters from the global fits are reported. Equilibrium constants are calculated from models. The value ‘Req/Rmax’ is reported as fraction  $Y_E$  bound.

### Exonuclease footprinting

Nucleic acid scaffolds used in exonuclease footprinting assays were each comprised of: (i) a  $^{32}\text{P}$ -labeled template DNA oligo, (ii) a non-template DNA oligo with four consecutive phosphorothioate bonds at

the 3' end, and (iii) an RNA oligo with 3' end at the position of pausing in *ops<sub>X</sub>* and having noncomplementary bases upstream of the RNA-DNA hybrid to prohibit backtracking.

Template DNA oligo (20  $\mu$ M) was labeled in a T4 PNK reaction with 1  $\mu$ Ci of [ $\gamma$ - $^{32}\text{P}$ ]ATP and allowed to proceed for 15 mins at  $37^{\circ}\text{C}$ . ATP (1  $\mu$ L of 1 mM) was subsequently added to the reaction and allowed to proceed for 30 min at  $37^{\circ}\text{C}$ . Reactions were stopped by heating at  $65^{\circ}\text{C}$  for 20 min and oligos were subsequently purified using G-50 columns pre-equilibrated with TE and following the manufacturer's instructions.

TECs were reconstituted essentially as described in in vitro transcription assays, except that the molar ratio of T:R:Pol:NT was 1:2:3:5 (50 nM  $^{32}\text{P}$ -T: 100 nM R: 150 nM RNAP: 250 nM NT). TECs were subsequently split into 35  $\mu$ L aliquots and incubated with either storage buffer or  $Y_X$  variants for 3 min at  $37^{\circ}\text{C}$ . Tubes were shifted to  $30^{\circ}\text{C}$  and allowed to incubate for 3 min before removing a 5  $\mu$ L aliquot (time 0) and mixing with equal volume 2 $\times$  Stop Buffer. Exonuclease reactions were initiated by adding 100  $\mu$ L of ExoIII, and aliquots were removed from reactions and mixed with stop buffer at times indicated in figures.

To quantify both transient and stable protection from exonuclease cleavage, pseudodensitometry traces were generated for the first timepoint lane. Regions of interest were identified by comparison to a sequencing ladder. Areas under the peaks of these regions were determined by manual integration in Microsoft Excel, then divided by the sum of the areas under all peaks to the right of it. These values were determined in the absence or presence of  $Y_B$ , and their ratio is reported as fold change ( $+Y_B/-Y_B$ ) for each sequence variant.

### Structural models

A model of  $Y_B$  was made using Modeller<sup>94,95</sup> and fitted to 8PHK<sup>33</sup>. Additional upstream and downstream DNA were modeled using Pymol. The  $Y_E$ - $Z_A$  complex structure was predicted using AlphaFold<sup>34</sup>, yielding an interface predicted template modeling (iPTM) score of 0.89 and predicted template modeling (pTM) score of 0.9 (values above 0.8 represent confident high-quality predictions). Additional confidence metrics are illustrated in Supplementary Fig. 6. RNA secondary structures were predicted using RNAFold<sup>95</sup>.

The *Bfr*RNA polymerase PEC model was generated using Modeller<sup>96</sup>, the *M. tuberculosis* PEC formed on the *B. subtilis* *trpL* pause sequence (8E74)<sup>27</sup>, NusA and NusG NGN models from SWISS-MODEL<sup>97</sup>, and *Porphyromonas gingivalis* RNAP (8DKC)<sup>98</sup>.

### Reporting summary

Further information on research design is available in the Nature Portfolio Reporting Summary linked to this article.

### Data availability

The NET-seq data generated in this study have been deposited in the NCBI GEO database under accession code GSE281607. The  $Y_E$ - $Z_A$  model generated by AlphaFold3 is available on Zenodo at <https://doi.org/10.5281/zenodo.14110860>. Source data are provided with this paper for all other experiments. Source data are provided with this paper.

### Code availability

Scripts for analyzing NET-seq data are available on Zenodo at <https://doi.org/10.5281/zenodo.14110860>.

### References

- Deng, H. et al. Bacteroides fragilis prevents clostridium difficile infection in a mouse model by restoring gut barrier and microbiome regulation. *Front. Microbiol.* **9**, 2976 (2018).
- Li, X. et al. A strain of Bacteroides thetaiotaomicron attenuates colonization of Clostridioides difficile and affects intestinal

- microbiota and bile acids profile in a mouse model. *Biomed. Pharmacother.* **137**, 111290 (2021).
3. Carasso, S. et al. Inflammation and bacteriophages affect DNA inversion states and functionality of the gut microbiota. *Cell Host Microbe* **32**, 322–334.e329 (2024).
  4. Hryckowian, A. J. et al. Bacteroides thetaiotaomicron-infecting bacteriophage isolates inform sequence-based host range predictions. *Cell Host Microbe* **28**, 371–379.e375 (2020).
  5. Porter, N. T. et al. Phase-variable capsular polysaccharides and lipoproteins modify bacteriophage susceptibility in Bacteroides thetaiotaomicron. *Nat. Microbiol.* **5**, 1170–1181 (2020).
  6. Bechon, N. et al. Capsular polysaccharide cross-regulation modulates bacteroides thetaiotaomicron biofilm formation. *mBio* **11** (2020). <https://doi.org/10.1128/mBio.00729-20>.
  7. Jiang, X. et al. Invertible promoters mediate bacterial phase variation, antibiotic resistance, and host adaptation in the gut. *Science* **363**, 181–187 (2019).
  8. Mazmanian, S. K., Liu, C. H., Tzianabos, A. O. & Kasper, D. L. An immunomodulatory molecule of symbiotic bacteria directs maturation of the host immune system. *Cell* **122**, 107–118 (2005).
  9. Mazmanian, S. K., Round, J. L. & Kasper, D. L. A microbial symbiosis factor prevents intestinal inflammatory disease. *Nature* **453**, 620–625 (2008).
  10. Porter, N. T., Canales, P., Peterson, D. A. & Martens, E. C. A subset of polysaccharide capsules in the human symbiont bacteroides thetaiotaomicron promote increased competitive fitness in the mouse gut. *Cell Host Microbe* **22**, 494–506.e498 (2017).
  11. Ramakrishna, C. et al. Bacteroides fragilis polysaccharide A induces IL-10 secreting B and T cells that prevent viral encephalitis. *Nat. Commun.* **10**, 2153 (2019).
  12. Chatzidakis-Livanis, M., Coyne, M. J. & Comstock, L. E. A family of transcriptional antitermination factors necessary for synthesis of the capsular polysaccharides of Bacteroides fragilis. *J. Bacteriol.* **191**, 7288–7295 (2009).
  13. Chatzidakis-Livanis, M., Weinacht, K. G. & Comstock, L. E. Trans locus inhibitors limit concomitant polysaccharide synthesis in the human gut symbiont Bacteroides fragilis. *Proc. Natl. Acad. Sci. USA* **107**, 11976–11980 (2010).
  14. Troy, E. B., Carey, V. J., Kasper, D. L. & Comstock, L. E. Orientations of the Bacteroides fragilis capsular polysaccharide biosynthesis locus promoters during symbiosis and infection. *J. Bacteriol.* **192**, 5832–5836 (2010).
  15. Lan, F. et al. Single-cell analysis of multiple invertible promoters reveals differential inversion rates as a strong determinant of bacterial population heterogeneity. *Sci. Adv.* **9**, eadg5476 (2023).
  16. Lan, F. et al. Massively parallel single-cell sequencing of diverse microbial populations. *Nat. Methods* **21**, 228–235 (2024).
  17. Coyne, M. J., Weinacht, K. G., Krinos, C. M. & Comstock, L. E. Mpi recombinase globally modulates the surface architecture of a human commensal bacterium. *Proc. Natl. Acad. Sci. USA* **100**, 10446–10451 (2003).
  18. Werner, F. A nexus for gene expression-molecular mechanisms of Spt5 and NusG in the three domains of life. *J. Mol. Biol.* **417**, 13–27 (2012).
  19. Bailey, M. J., Koronakis, V., Schmoll, T. & Hughes, C. Escherichia coli HlyT protein, a transcriptional activator of haemolysin synthesis and secretion, is encoded by the rfaH (sfrB) locus required for expression of sex factor and lipopolysaccharide genes. *Mol. Microbiol.* **6**, 1003–1012 (1992).
  20. Bies-Etheve, N. et al. RNA-directed DNA methylation requires an AGO4-interacting member of the SPT5 elongation factor family. *EMBO Rep.* **10**, 649–654 (2009).
  21. Goodson, J. R., Klupt, S., Zhang, C., Straight, P. & Winkler, W. C. LoaP is a broadly conserved antiterminator protein that regulates antibiotic gene clusters in Bacillus amyloliquefaciens. *Nat. Microbiol.* **2**, 17003 (2017).
  22. Artsimovitch, I. & Landick, R. The transcriptional regulator RfaH stimulates RNA chain synthesis after recruitment to elongation complexes by the exposed non-template DNA strand. *Cell* **109**, 193–203 (2002).
  23. Kang, J. Y. et al. Structural basis for transcript elongation control by NusG/RfaH universal regulators. *Cell* **173**, 1650–1662.e1614 (2018).
  24. Leeds, J. A. & Welch, R. A. RfaH enhances elongation of Escherichia coli hlyCABD mRNA. *J. Bacteriol.* **178**, 1850–1857 (1996).
  25. Yakhnin, A. V. et al. Robust regulation of transcription pausing in Escherichia coli by the ubiquitous elongation factor NusG. *Proc. Natl. Acad. Sci. USA* **120**, e2221114120 (2023).
  26. Czyz, A., Mooney, R. A., Iaconi, A. & Landick, R. Mycobacterial RNA polymerase requires a U-tract at intrinsic terminators and is aided by NusG at suboptimal terminators. *mBio* **5**, e00931 (2014).
  27. Delbeau, M. et al. Structural and functional basis of the universal transcription factor NusG pro-pausing activity in Mycobacterium tuberculosis. *Mol. Cell* **83**, 1474–1488.e1478 (2023).
  28. Mandell, Z. F. et al. NusG is an intrinsic transcription termination factor that stimulates motility and coordinates gene expression with NusA. *Elife* **10** (2021). <https://doi.org/10.7554/eLife.61880>.
  29. Mondal, S., Yakhnin, A. V., Sebastian, A., Albert, I. & Babitzke, P. NusA-dependent transcription termination prevents misregulation of global gene expression. *Nat. Microbiol.* **1**, 15007 (2016).
  30. Sevostyanova, A. & Artsimovitch, I. Functional analysis of Thermus thermophilus transcription factor NusG. *Nucleic Acids Res.* **38**, 7432–7445 (2010).
  31. Landick, R. Transcriptional pausing as a mediator of bacterial gene regulation. *Annu. Rev. Microbiol.* **75**, 291–314 (2021).
  32. Zuber, P. K. et al. The universally-conserved transcription factor RfaH is recruited to a hairpin structure of the non-template DNA strand. *Elife* **7** (2018). <https://doi.org/10.7554/eLife.36349>.
  33. Zuber, P. K. et al. Concerted transformation of a hyper-paused transcription complex and its reinforcing protein. *Nat. Commun.* **15**, 3040 (2024).
  34. Paitan, Y., Orr, E., Ron, E. Z. & Rosenberg, E. A NusG-like transcription anti-terminator is involved in the biosynthesis of the polyketide antibiotic TA of Myxococcus xanthus. *FEMS Microbiol. Lett.* **170**, 221–227 (1999).
  35. Nunez, B., Avila, P. & de la Cruz, F. Genes involved in conjugative DNA processing of plasmid R6K. *Mol. Microbiol.* **24**, 1157–1168 (1997).
  36. Churchman, L. S. & Weissman, J. S. Nascent transcript sequencing visualizes transcription at nucleotide resolution. *Nature* **469**, 368–373 (2011).
  37. Larson, M. H. et al. A pause sequence enriched at translation start sites drives transcription dynamics in vivo. *Science* **344**, 1042–1047 (2014).
  38. Artsimovitch, I. & Landick, R. Pausing by bacterial RNA polymerase is mediated by mechanistically distinct classes of signals. *Proc. Natl. Acad. Sci. USA* **97**, 7090–7095 (2000).
  39. Guo, X. et al. Structural basis for NusA stabilized transcriptional pausing. *Mol. Cell* **69**, 816–827.e814 (2018).
  40. Kang, J. Y. et al. RNA polymerase accommodates a pause RNA hairpin by global conformational rearrangements that prolong pausing. *Mol. Cell* **69**, 802–815.e805 (2018).
  41. Krinos, C. M. et al. Extensive surface diversity of a commensal microorganism by multiple DNA inversions. *Nature* **414**, 555–558 (2001).
  42. Daube, S. S. & von Hippel, P. H. Functional transcription elongation complexes from synthetic RNA-DNA bubble duplexes. *Science* **258**, 1320–1324 (1992).
  43. Toulkhourov, I., Artsimovitch, I. & Landick, R. Allosteric control of RNA polymerase by a site that contacts nascent RNA hairpins. *Science* **292**, 730–733 (2001).

44. Bao, Y., Cao, X. & Landick, R. RNA polymerase SI3 domain modulates global transcriptional pausing and pause-site fluctuations. *Nucleic Acids Res.* (2024). <https://doi.org/10.1093/nar/gkae209>.
45. Gajos, M. et al. Conserved DNA sequence features underlie pervasive RNA polymerase pausing. *Nucleic Acids Res.* **49**, 4402–4420 (2021).
46. Kireeva, M. L. & Kashlev, M. Mechanism of sequence-specific pausing of bacterial RNA polymerase. *Proc. Natl. Acad. Sci. USA* **106**, 8900–8905 (2009).
47. Yakhnin, A. V. et al. NusG controls transcription pausing and RNA polymerase translocation throughout the *Bacillus subtilis* genome. *Proc. Natl. Acad. Sci. USA* **117**, 21628–21636 (2020).
48. Ha, K. S., Touloukionov, I., Vassilyev, D. G. & Landick, R. The NusA N-terminal domain is necessary and sufficient for enhancement of transcriptional pausing via interaction with the RNA exit channel of RNA polymerase. *J. Mol. Biol.* **401**, 708–725 (2010).
49. Jayasinghe, O. T., Mandell, Z. F., Yakhnin, A. V., Kashlev, M. & Babitzke, P. Transcriptome-wide effects of NusA on RNA polymerase pausing in *Bacillus subtilis*. *J. Bacteriol.* **204**, e0053421 (2022).
50. Kolb, K. E., Hein, P. P. & Landick, R. Antisense oligonucleotide-stimulated transcriptional pausing reveals RNA exit channel specificity of RNA polymerase and mechanistic contributions of NusA and RfaH. *J. Biol. Chem.* **289**, 1151–1163 (2014).
51. Strobel, E. J. & Roberts, J. W. Two transcription pause elements underlie a sigma70-dependent pause cycle. *Proc. Natl. Acad. Sci. USA* **112**, e4374–e4380 (2015).
52. Revyakin, A., Liu, C., Ebright, R. H. & Strick, T. R. Abortive initiation and productive initiation by RNA polymerase involve DNA scrunching. *Science* **314**, 1139–1143 (2006).
53. Roberts, J. W. Biochemistry. RNA polymerase, a scrunching machine. *Science* **314**, 1097–1098 (2006).
54. Abramson, J. et al. Accurate structure prediction of biomolecular interactions with AlphaFold 3. *Nature* (2024). <https://doi.org/10.1038/s41586-024-07487-w>.
55. Elghondakly, A., Wu, C. H., Klupt, S., Goodson, J. & Winkler, W. C. A NusG Specialized Paralog That Exhibits Specific, High-Affinity RNA-Binding Activity. *J. Mol. Biol.* **433**, 167100 (2021).
56. Eckart, K. A. et al. Compensatory evolution in NusG improves fitness of drug-resistant *M. tuberculosis*. *Nature* (2024). <https://doi.org/10.1038/s41586-024-07206-5>.
57. Sevostyanova, A., Belogurov, G. A., Mooney, R. A., Landick, R. & Artsimovitch, I. The beta subunit gate loop is required for RNA polymerase modification by RfaH and NusG. *Mol. Cell* **43**, 253–262 (2011).
58. You, L. et al. Structural basis for intrinsic transcription termination. *Nature* **613**, 783–789 (2023).
59. Zhu, C. et al. Transcription factors modulate RNA polymerase conformational equilibrium. *Nat. Commun.* **13**, 1546 (2022).
60. Harteis, S. & Schneider, S. Making the bend: DNA tertiary structure and protein-DNA interactions. *Int. J. Mol. Sci.* **15**, 12335–12363 (2014).
61. Landick, R. & Yanofsky, C. Isolation and structural analysis of the *Escherichia coli* trp leader paused transcription complex. *J. Mol. Biol.* **196**, 363–377 (1987).
62. Nedialkov, Y., Svetlov, D., Belogurov, G. A. & Artsimovitch, I. Locking the non-template DNA to control transcription. *Mol. Microbiol.* **109**, 445–457 (2018).
63. Samkurashvili, I. & Luse, D. S. Translocation and transcriptional arrest during transcript elongation by RNA polymerase II. *J. Biol. Chem.* **271**, 23495–23505 (1996).
64. Lane, W. J. & Darst, S. A. Molecular evolution of multisubunit RNA polymerases: sequence analysis. *J. Mol. Biol.* **395**, 671–685 (2010).
65. Cao, X. et al. Basis of narrow-spectrum activity of fidaxomicin on *Clostridioides difficile*. *Nature* **604**, 541–545 (2022).
66. Vishwakarma, R. K., Qayyum, M. Z., Babitzke, P. & Murakami, K. S. Allosteric mechanism of transcription inhibition by NusG-dependent pausing of RNA polymerase. *Proc. Natl. Acad. Sci. USA* **120**, e2218516120 (2023).
67. Hustmyer, C. M., Wolfe, M. B., Welch, R. A. & Landick, R. RfaH counter-silences inhibition of transcript elongation by H-Ns-StpA nucleoprotein filaments in pathogenic *Escherichia coli*. *mBio* **13**, e0266222 (2022).
68. Accetto, T. & Avgustin, G. Inability of *Prevotella bryantii* to form a functional Shine-Dalgarno interaction reflects unique evolution of ribosome binding sites in Bacteroidetes. *PLoS ONE* **6**, e22914 (2011).
69. Mastropaolo, M. D., Thorson, M. L. & Stevens, A. M. Comparison of *Bacteroides thetaiotaomicron* and *Escherichia coli* 16S rRNA gene expression signals. *Microbiology* **155**, 2683–2693 (2009).
70. Mimee, M., Tucker, A. C., Voigt, C. A. & Lu, T. K. Programming a Human Commensal Bacterium, *Bacteroides thetaiotaomicron*, to Sense and Respond to Stimuli in the Murine Gut Microbiota. *Cell Syst.* **1**, 62–71 (2015).
71. Wegmann, U., Horn, N. & Carding, S. R. Defining the bacteroides ribosomal binding site. *Appl. Environ. Microbiol.* **79**, 1980–1989 (2013).
72. Johnson, G. E., Lalanne, J. B., Peters, M. L. & Li, G. W. Functionally uncoupled transcription-translation in *Bacillus subtilis*. *Nature* **585**, 124–128 (2020).
73. Adhya, S. & Gottesman, M. Control of transcription termination. *Annu. Rev. Biochem.* **47**, 967–996 (1978).
74. Burmann, B. M. et al. A NusE:NusG complex links transcription and translation. *Science* **328**, 501–504 (2010).
75. Byrne, R., Levin, J. G., Bladen, H. A. & Nirenberg, M. W. The in vitro formation of a DNA-Ribosome complex. *Proc. Natl. Acad. Sci. USA* **52**, 140–148 (1964).
76. Castro-Roa, D. & Zenkin, N. In vitro experimental system for analysis of transcription-translation coupling. *Nucleic acids Res.* **40**, e45 (2012).
77. Landick, R., Carey, J. & Yanofsky, C. Translation activates the paused transcription complex and restores transcription of the trp operon leader region. *Proc. Natl. Acad. Sci. USA* **82**, 4663–4667 (1985).
78. McGary, K. & Nudler, E. RNA polymerase and the ribosome: the close relationship. *Curr. Opin. Microbiol.* **16**, 112–117 (2013).
79. Miller, O. L. Jr, Hamkalo, B. A. & Thomas, C. A. Jr Visualization of bacterial genes in action. *Science* **169**, 392–395 (1970).
80. Proshkin, S., Rahmouni, A. R., Mironov, A. & Nudler, E. Cooperation between translating ribosomes and RNA polymerase in transcription elongation. *Science* **328**, 504–508 (2010).
81. Saxena, S. et al. *Escherichia coli* transcription factor NusG binds to 70S ribosomes. *Mol. Microbiol.* **108**, 495–504 (2018).
82. Stevenson-Jones, F., Woodgate, J., Castro-Roa, D. & Zenkin, N. Ribosome reactivates transcription by physically pushing RNA polymerase out of transcription arrest. *Proc. Natl. Acad. Sci. USA* **117**, 8462–8467 (2020).
83. Burmann, B. M. et al. An alpha helix to beta barrel domain switch transforms the transcription factor RfaH into a translation factor. *Cell* **150**, 291–303 (2012).
84. Lorber, C. G. [Differential diagnosis of maxillofacial neuralgia]. *ZWR* **85**, 514–518 (1976).
85. O'Donnell, S. M. & Janssen, G. R. The initiation codon affects ribosome binding and translational efficiency in *Escherichia coli* of cl mRNA with or without the 5' untranslated leader. *J. Bacteriol.* **183**, 1277–1283 (2001).
86. Jin, D. J. & Gross, C. A. Mapping and sequencing of mutations in the *Escherichia coli* rpoB gene that lead to rifampicin resistance. *J. Mol. Biol.* **202**, 45–58 (1988).
87. Pantosti, A., Tzianabos, A. O., Onderdonk, A. B. & Kasper, D. L. Immunochemical characterization of two surface polysaccharides of *Bacteroides fragilis*. *Infect. Immun.* **59**, 2075–2082 (1991).
88. Garcia-Bayona, L. & Comstock, L. E. Streamlined genetic manipulation of diverse bacteroides and parabacteroides isolates from



- the human gut microbiota. *mBio* **10** (2019). <https://doi.org/10.1128/mBio.01762-19>.
89. Welch, M. et al. Design parameters to control synthetic gene expression in *Escherichia coli*. *PLoS ONE* **4**, e7002 (2009).
  90. Windgassen, T. A. et al. Trigger-helix folding pathway and S13 mediate catalysis and hairpin-stabilized pausing by *Escherichia coli* RNA polymerase. *Nucleic Acids Res.* **42**, 12707–12721 (2014).
  91. Reis, A. C. & Salis, H. M. An automated model test system for systematic development and improvement of gene expression models. *ACS Synth. Biol.* **9**, 3145–3156 (2020).
  92. Salis, H. M., Mirsky, E. A. & Voigt, C. A. Automated design of synthetic ribosome binding sites to control protein expression. *Nat. Biotechnol.* **27**, 946–950 (2009).
  93. Saba, J. et al. The elemental mechanism of transcriptional pausing. *Elife* **8** (2019). <https://doi.org/10.7554/eLife.40981>.
  94. Sali, A. & Blundell, T. L. Comparative protein modelling by satisfaction of spatial restraints. *J. Mol. Biol.* **234**, 779–815 (1993).
  95. Gruber, A. R., Lorenz, R., Bernhart, S. H., Neubock, R. & Hofacker, I. L. The Vienna RNA websuite. *Nucleic Acids Res.* **36**, W70–W74 (2008).
  96. Webb, B. & Sali, A. Comparative protein structure modeling using MODELLER. *Curr. Protoc. Bioinforma.* **54**, 5 6 1–5 6 37 (2016).
  97. Waterhouse, A. et al. SWISS-MODEL: homology modelling of protein structures and complexes. *Nucleic Acids Res.* **46**, W296–W303 (2018).
  98. Bu, F. et al. Cryo-EM structure of *Porphyromonas gingivalis* RNA polymerase. *J. Mol. Biol.* **436**, 168568 (2024).
  99. Coyne, M. J. et al. Polysaccharide biosynthesis locus required for virulence of *Bacteroides fragilis*. *Infect. Immun.* **69**, 4342–4350 (2001).
  100. Sultana, A. & Lee, J. E. Measuring protein-protein and protein-nucleic acid interactions by biolayer interferometry. *Curr. Protoc. Protein Sci.* **79**, 19 25 11–19 25 26 (2015).
  101. Madeira, F. et al. The EMBL-EBI job dispatcher sequence analysis tools framework in 2024. *Nucleic Acids Res.* (2024). <https://doi.org/10.1093/nar/gkae241>.

## Acknowledgements

We thank members of the Landick and Comstock labs for helpful discussions and comments on the manuscript. This work was supported by NIH R01 GM038660 and USDA Hatch WIS05004 to R.L., NIH R01 AI093771 to L.C., the Duchossois Family Institute, and the DOE Office of Science, Biological and Environmental Research Program Great Lakes Bioenergy Research Center (DE-SC0018409). A.G. was supported by the NIH Predoctoral Training Program in Genetics (T32 GM007133). J.S. was supported by the NIH Biotechnology Training Grant (T32 GM135066 and T32 GM008349), an NIH F31 Graduate Fellowship (F31 GM142153), and a SciMed Graduate Research Scholars Fellowship from the UW–Madison Graduate School and Wisconsin Alumni Research Foundation.

## Author contributions

R.L. and J.S. conceived of the study. J.S. conceived and developed assays, cloned most plasmids, purified all proteins, performed most experiments, and analyzed data. K.F. constructed plasmids for *B. fragilis* genetic manipulation, created *Bacteroides* strains and performed Western blots. M.E., B.M., and J.S. wrote custom scripts. J.S. and R.L. interpreted data. M.E., Y.P., and A.G. performed experiments. R.L. and J.S. constructed structural models. J.S. and R.L. wrote the original manuscript and designed figures. J.S., R.L., and L.C. revised the manuscript. R.L., L.C., and J.S., secured funding. R.L. and L.C. supervised the study.

## Competing interests

The authors declare no competing interests.

## Additional information

**Supplementary information** The online version contains supplementary material available at <https://doi.org/10.1038/s41467-024-55215-9>.

**Correspondence** and requests for materials should be addressed to Robert Landick.

**Peer review information** *Nature Communications* thanks the anonymous reviewers for their contribution to the peer review of this work. A peer review file is available.

**Reprints and permissions information** is available at <http://www.nature.com/reprints>

**Publisher's note** Springer Nature remains neutral with regard to jurisdictional claims in published maps and institutional affiliations.

**Open Access** This article is licensed under a Creative Commons Attribution-NonCommercial-NoDerivatives 4.0 International License, which permits any non-commercial use, sharing, distribution and reproduction in any medium or format, as long as you give appropriate credit to the original author(s) and the source, provide a link to the Creative Commons licence, and indicate if you modified the licensed material. You do not have permission under this licence to share adapted material derived from this article or parts of it. The images or other third party material in this article are included in the article's Creative Commons licence, unless indicated otherwise in a credit line to the material. If material is not included in the article's Creative Commons licence and your intended use is not permitted by statutory regulation or exceeds the permitted use, you will need to obtain permission directly from the copyright holder. To view a copy of this licence, visit <http://creativecommons.org/licenses/by-nc-nd/4.0/>.

© The Author(s) 2024